Rab21 in enterocytes participates in intestinal epithelium maintenance

Sonya Nassari, Camille Lacarrière-Keïta, Dominique Lévesque, François-Michel Boisvert, and Steve Jean*
Department of Immunology and Cell Biology, Faculté de Médecine et des Sciences de la Santé, Université de Sherbrooke, Sherbrooke, Québec J1E 4K8, Canada

ABSTRACT Membrane trafficking is defined as the vesicular transport of proteins into, out of, and throughout the cell. In intestinal enterocytes, defects in endocytic/recycling pathways result in impaired function and are linked to diseases. However, how these trafficking pathways regulate intestinal tissue homeostasis is poorly understood. Using the *Drosophila* intestine as an in vivo system, we investigated enterocyte-specific functions for the early endosomal machinery. We focused on Rab21, which regulates specific steps in early endosomal trafficking. Depletion of Rab21 in enterocytes led to abnormalities in intestinal morphology, with deregulated cellular equilibrium associated with a gain in mitotic cells and increased cell death. Increases in apoptosis and Yorkie signaling were responsible for compensatory proliferation and tissue inflammation. Using an RNA interference screen, we identified regulators of autophagy and membrane trafficking that phenocopied *Rab21* knockdown. We further showed that *Rab21* knockdown-induced hyperplasia was rescued by inhibition of epidermal growth factor receptor signaling. Moreover, quantitative proteomics identified proteins affected by Rab21 depletion. Of these, we validated changes in apolipoprotein ApoLpp and the trehalose transporter Tret1-1, indicating roles for enterocyte Rab21 in lipid and carbohydrate homeostasis, respectively. Our data shed light on an important role for early endosomal trafficking, and Rab21, in enterocyte-mediated intestinal epithelium maintenance.

INTRODUCTION

Membrane trafficking is characterized by the vesicular transport of proteins and macromolecules throughout the various cellular compartments, as well as in and out of cells. This process requires exchanges between compartments that are essential to maintain cellular functions and help cells adapt to the ever-changing conditions in the extra- and intracellular environments. The intricate link between membrane trafficking and cellular signaling means that modulating trafficking has strong consequences on cellular homeostasis (Nassari *et al.*, 2020). Mutations in different membrane trafficking genes are responsible for a large array of human diseases (Yarwood *et al.*, 2020) that impair various tissues to different degrees. Importantly, some of these mutations have systemic effects, while others impact specific tissues (Yarwood *et al.*, 2020).

The digestive tract performs several essential functions, including food digestion, nutrient/water absorption, and protection against external pathogens. These tasks are performed by entero-

cytes, a differentiated cell population constituting ~80% of the intestinal epithelium. Given their absorptive function, enterocytes display high membrane trafficking flux, which must be tightly orchestrated to ensure appropriate organ activity (Engevik and Goldenring, 2018). Defects in trafficking processes affect enterocyte properties (e.g., their shape, absorptive function, and resistance to stress) and lead to intestinal diseases (Sato *et al.*, 2007; Engevik and Goldenring, 2018). Intestinal pathologies, such as microvillus inclusions and chylomicron retention disease, are associated with mutations in the membrane trafficking–related genes *MYO5B* and syntaxin 3 (*STX3*) (Müller *et al.*, 2008; Wiegerinck *et al.*, 2014) and secretion-associated Ras-related GTPase 1B (*SAR1B*), respectively (Müller *et al.*, 2008; Sané *et al.*, 2017; Yarwood *et al.*, 2020). STX3 is important for apical vesicle fusion to the membrane (Wiegerinck *et al.*, 2014), MYO5B is required for proper recycling to the apical membrane (Müller *et al.*, 2008), and SAR1B is necessary for chylomicron secretion (Sané *et al.*, 2017).

The small Rab GTPases constitute an important class of membrane trafficking regulators (Jean and Kiger, 2012). Rabs localize to specific cellular compartments, where they recruit various effectors to mediate their functions. In enterocytes, a few studies have reported the involvement of Rab8a and Rab11a, both components of the endosomal recycling machinery, in the regulation of apical brush border formation (Sato *et al.*, 2007; Knowles *et al.*, 2015; Engevik and Goldenring, 2018). In *Rab8a*-knockout mice, apical peptidases and transporters accumulate in lysosomes. This leads to decreased absorptive functions, which are associated with microvillus inclusion and defects in microvillar structure (Sato *et al.*, 2007). Similarly, mice deficient for enterocyte cell division cycle 42 (*Cdc42*), which is important for Rab8a activation, display microvilli inclusions (Sakamori *et al.*, 2012; Melendez *et al.*, 2013), and restricted apical localization of Cdc42 is affected in microvilli inclusion diseases (Michaux *et al.*, 2016). Loss of *Rab11a* in mouse intestinal epithelial cells results in defects in enterocyte polarity and abnormal microvilli organization (Knowles *et al.*, 2015; Feng *et al.*, 2017). Notably, the enterocyte polarity defect upon *Rab11* knockdown is conserved in *Drosophila* (Nie *et al.*, 2019). In the *Caenorhabditis elegans* intestine, Rab11 also displays an apical distribution, which is required to establish proper polarity in intestinal epithelial cells (Winter *et al.*, 2012). Another study demonstrated roles for Rab11 in toll-like receptor regulation and microbial tolerance in mouse and *Drosophila* intestines (Yu *et al.*, 2014). Finally, recent research performed in mice and flies highlighted a conserved role for Rab11 in intestinal tumor progression via regulation of the Hippo pathway (D'Agostino *et al.*, 2019). Although roles for the endosomal recycling machinery in enterocytes have been well documented, little is known about the functions of other membrane trafficking routes in these cells and, more generally, in intestinal tissue homeostasis.

Early endosomes act as sorting centers, in which endocytosed cargoes must be correctly directed toward either recycling routes or lysosomal degradation (Cullen and Steinberg, 2018). Therefore, early endosomes are important for proper regulation of internalized signals (Nassari *et al.*, 2020). Rab5 is often associated with early endosomes, where it acts in endosomal homotypic fusion and in endocytosis (Galvez *et al.*, 2012). Rab5 is also necessary for phosphatidylinositol-3-phosphate (PtdIns(3)P) synthesis in early endosomes (Shin *et al.*, 2005). In flies, Rab5 is required for proper localization of apical proteins in polarized epithelia (Lu and Bilder, 2005; Morrison *et al.*, 2008). In contrast, in mice, Rab5 is required for lysosomal homeostasis in the liver (Zeigerer *et al.*, 2012). Several other Rabs are also present in early endosomes (Hutagalung

and Novick, 2011), including Rab21, which is involved in endocytosis and early endosomal trafficking of integrins, epidermal growth factor receptor (EGFR), and certain clathrin-independent cargoes (Pellinen *et al.*, 2006; Jean *et al.*, 2012; Del Olmo *et al.*, 2019; Moreno-Layseca *et al.*, 2021). Rab21 was first identified in human intestinal Caco-2 cells (Opdam *et al.*, 2000). Upon Caco-2 cell polarization, Rab21's cytoplasmic distribution changes, restricting it to the apical side of differentiated cells. Similarly, Rab21 is expressed in epithelial cells in both human and mouse intestines, with apical enrichment (Opdam *et al.*, 2000; Zhang *et al.*, 2016), and is highly expressed in the villi of both humans and mice, with only weak expression in the crypts. This suggests a specific function for Rab21 in differentiated intestinal epithelial cells. Interestingly, a recent study demonstrated that Rab21 expression is decreased in enterocytes in solute carrier family 15 (oligopeptide transporter), member 1 (*Slc15a1*)-knockout mice (Zhang *et al.*, 2016), with *Slc15a1* being a susceptibility variant gene for inflammatory bowel disease (IBD) (Ayyadurai *et al.*, 2013; Viennois *et al.*, 2016).

These data led us to investigate the specific functions of Rab21 and other trafficking regulators in enterocytes in vivo, using the *Drosophila* intestine as a model system. *Drosophila* enables the use of powerful genetic tools and is an excellent model to investigate intestinal biology, with intestinal signaling pathways and functions highly similar to those of humans (Miguel-Aliaga *et al.*, 2018). Like the mammalian intestine, the *Drosophila* digestive tract is composed of intestinal stem cells that differentiate into progenitor cells that yield differentiated enteroendocrine cells and enterocytes (Micchelli and Perrimon, 2006; Ohlstein and Spradling, 2006; Miguel-Aliaga *et al.*, 2018). The coordination of several signaling pathways orchestrates the balance between intestinal stem cell proliferation, progenitor differentiation, and differentiated cell turnover. Under normal conditions, Wnt signaling is required for intestinal stem cell self-renewal, similar to mammals (Lin and Xi, 2008; Lin *et al.*, 2008), while high levels of Notch signaling in progenitor cells promote enterocyte differentiation (Micchelli and Perrimon, 2006; Ohlstein and Spradling, 2006). Upon stress, the Janus kinase-signal transducer and activator of transcription (JAK-STAT), EGFR, c-Jun NH(2)-terminal kinase (JNK), and Hippo signaling pathways activate intestinal stem cell proliferation and progenitor differentiation in response to various injuries (Jiang and Edgar, 2011). Furthermore, upon intestinal epithelial stress, enterocytes serve as stress sensors to initiate tissue regeneration and rapidly compensate for cell loss by promoting the non–cell autonomous activation of intestinal stem cells. The JNK and Hippo/Yorkie (Yki) pathways are involved in this process in enterocytes, where they trigger expression of the proinflammatory cytokine Unpaired 3 (Upd3) (Jiang *et al.*, 2009, 2011; Ren *et al.*, 2010; Shaw *et al.*, 2010; Staley and Irvine, 2010; Loudhaief *et al.*, 2017). Secretion of Upd3 promotes intestinal stem cell proliferation by directly activating the JAK-STAT pathway and indirectly activating EGFR signaling (Jiang *et al.*, 2009, 2011; Buchon *et al.*, 2010).

Here, we demonstrate that functional early endosomes are required for proper tissue organization in the fly midgut. Knockdown of *Rab21* in *Drosophila* enterocytes results in Yki activation and apoptosis, both of which induce secretion of the proinflammatory cytokine Upd3, leading to compensatory proliferation in a non–cell autonomous manner. An enterocyte-focused screen of membrane trafficking genes reveals that blocking autophagy, endosomal trafficking, or EGFR-mitogen–activated protein kinase (MAPK) signaling activation also induces tissue inflammation and hyperproliferation. Using epistasis experiments, we show that Rab21 regulates enterocyte EGFR signaling and autophagy independently.

Additionally, we highlight a previously unappreciated contribution of Rab21 in PtdIns(3)P and PtdIns(3,5)P_2 regulation. Finally, using a tandem mass tag (TMT)-based quantitative proteomics approach we reveal the deregulation of a broad range of proteins, many of them related to lipid and sugar metabolism. Consistent with this, we show that both of these metabolic pathways are affected in intestines depleted of Rab21 by RNA interference (RNAi).

RESULTS

Enterocyte Rab21 is required to maintain intestinal epithelium morphology

Fluorescence-activated cell-sorted and single-cell RNA-sequencing databases indicate that the early endosome components *Rab5* and *Rab21* and the recycling endosome component *Rab11* are expressed in various cell types throughout the fly intestine (Buchon *et al.*, 2013; Marianes and Spradling, 2013; Dutta *et al.*, 2015). *Rab21* is normally expressed at lower levels than *Rab5*; however, it is up-regulated upon infection. As the role of Rab11 in intestinal homeostasis is well-described (Engevik and Goldenring, 2018), we decided to focus our initial analysis on Rab21, which plays roles in specific early endosomal trafficking events (Pellinen *et al.*, 2006; Jean *et al.*, 2012, 2015; Yang *et al.*, 2012; Del Olmo *et al.*, 2019). However, no functions have been described for Rab21 in intestinal epithelial cells, despite its modulation in mouse models of IBD (Dutta *et al.*, 2015; Zhang et al., 2016).

We first determined Rab21's precise expression pattern in the *Drosophila* midgut using the Gal4-UAS expression system (Chan *et al.*, 2011). We used a *Rab21*-Gal4 driver line combined with UASt-green fluorescent protein (GFP):Rab21 responder line, resulting in GFP:Rab21 expression in an endogenous pattern. In accordance with transcriptomic data (Buchon *et al.*, 2013; Marianes and Spradling, 2013; Dutta *et al.*, 2015), we observed that Rab21 was present throughout the digestive tract (Figure 1, A and B), with differing expression levels among the three main regions of the midgut (Figure 1, A and B). Interestingly, Rab21 displayed stronger expression in the distal part of the posterior midgut (R5 region) (Dutta *et al.*, 2015) and in the copper cell region (Figure 1B). In the R5 region, Rab21 expression was enriched in large polyploid cells with low levels of Armadillo (Arm) staining, characteristic of enterocytes (Figure 1, C and D, arrowheads). Using *Rab21*-GAL4, UAS-GFP:*Rab21*^{WT} expressing flies, we did not detect apicobasal polarization of Rab21 (Supplemental Figure 1A). This could be due to amplified expression of GFP:Rab21 caused by the Gal4 reporter system. Using RNA in situ hybridization, we confirmed that *Rab21* was expressed in enterocytes in the posterior midgut, which were visualized with 4′,6-diamidino-2-phenylindole (DAPI) to highlight their polyploid nuclei (Supplemental Figure 1B). We also detected Rab21 in cells displaying high Arm staining, which were likely intestinal stem cells (Figure 1, C and D″, arrows). Immunofluorescence against Delta (Dl) confirmed that Rab21 was present in intestinal stem cells (Dl$^+$; Supplemental Figure 1C). Rab21 was also detected in Prospero (Pros)$^+$ cells (Supplemental Figure 1C), revealing that enteroendocrine cells also express Rab21. As previously observed in human and mouse intestines (Opdam *et al.*, 2000; Zhang *et al.*, 2016), these data show that Rab21 is expressed throughout the fly gut, with high expression in enterocytes, raising the possibility of important functions in these cells.

To characterize Rab21 functions in enterocytes, we interfered with its activity using a cell-specific inducible system (McGuire *et al.*, 2004). Two independent and previously validated (Jean *et al.*, 2012) *Rab21* RNAi hairpins and a dominant negative (DN) *Rab21* construct (*Rab21*^{DN}) (Jean *et al.*, 2012) were expressed only in the enterocytes

of adults using *Myo1A-Gal4, UAS GFP; tub-Gal80*^{ts}(hereafter referred to as *Myo1A*^{ts}) transgenic flies. Flies were housed at 18°C during embryonic development, switched to 29°C for 10 d after hatching, and then analyzed (Figure 1E). *Rab21* knockdown efficiency in enterocytes was confirmed for both RNAi hairpins by quantitative reverse transcription-PCR (qRT-PCR) and Western blotting (Supplemental Figure 2, A and B). Decreased Rab21 activity mediated by RNAi or Rab21-DN expression in enterocytes was associated with a significant increase in cell density (Figure 1F), indicating defects in tissue morphology. Consistent with this notion, compared with controls (Figure 1G; Supplemental Figure 2C), the organization of the cell junction markers Coracle (Cora; Figure 1G) and Armadillo (Arm; Supplemental Figure 2C) was disrupted with decreased Rab21 activity. Analysis of early time points (3 and 5 d) after RNAi induction in enterocytes did not reveal any common phenotypes affecting tissue organization (Supplemental Figure 2D). At 5 d, only *Rab21* RNAi-1 displayed abnormal cell junction staining (Supplemental Figure 2D). Because both RNAi lines induced similar defects at 10 d, we decided to analyze all experiments at that time point. In contrast to Rab11 depletion-related defects (Yu *et al.*, 2014), we did not observe noticeable changes in the microvillar structure or polarity of Rab21-depleted enterocytes (Supplemental Figure 2E), and Smurf assays revealed no defects in tissue permeability in flies expressing *Rab21* RNAi in enterocytes (Supplemental Figure 2F). Furthermore, *Rab21* knockdown in enterocytes led to a multilayered epithelium (Figure 1H; Supplemental Video 2), which was never observed in control flies (Figure 1H; Supplemental Video 1). Consistent with this observation, the intestinal lumen area tended to be reduced in flies expressing *Rab21* RNAi (Figure 1I). Importantly, overexpression of Rab21^{DN} in enterocytes had similar effects (Figure 1, F and G; Supplemental Figure 2D), supporting the specificity of the observed phenotypes. Survival experiments showed that interference with Rab21 function in enterocytes through either RNAi or Rab21^{DN} expression reduced lifespan (Figure 1J). Importantly, intestinal morphology defects observed with *Rab21* RNAi were suppressed by overexpression of an RNAi-insensitive *Rab21* construct referred to as *Rab21 degenerate* (*Rab21*^{deg}; Figure 1G), confirming the specificity of the *Rab21* RNAi reagents. Altogether, these results highlight the contribution of enterocyte Rab21 in the maintenance of midgut morphology and fly lifespan.

Enterocyte Rab21 maintains intestinal cellular equilibrium

Enterocytes are nonmitotic, terminally differentiated cells arising from progenitors produced by intestinal stem cells (Figure 2A). Surprisingly, Rab21 depletion from enterocytes resulted in supernumerary cells underneath the Myo1A$^+$ cells that were never observed in control intestines (Figure 2B). These cells did not express Myo1A, suggesting that they were not enterocytes. Furthermore, the percentage of Myo1A$^+$ cells was decreased in intestines expressing *Rab21* RNAi compared with controls (Figure 2C). To identify the accumulating cells, we assessed the impact of *Rab21* knockdown in enterocytes on the other main midgut cell types. Using immunofluorescence against Pros and Dl, respectively, we noticed increases in both the enteroendocrine cells and stem cell populations upon *Rab21* knockdown (Figure 2, D and E). The increased proportion of intestinal stem cells was further confirmed using a Dl:GFP reporter line (Figure 2E). From these data, we conclude that enterocyte Rab21 is necessary to maintain the normal ratio of cell types in the intestine.

Rab21 is necessary for proper cell turnover

Next, we investigated the signaling mechanisms impacting the various gut cell populations upon *Rab21* knockdown from enterocytes.
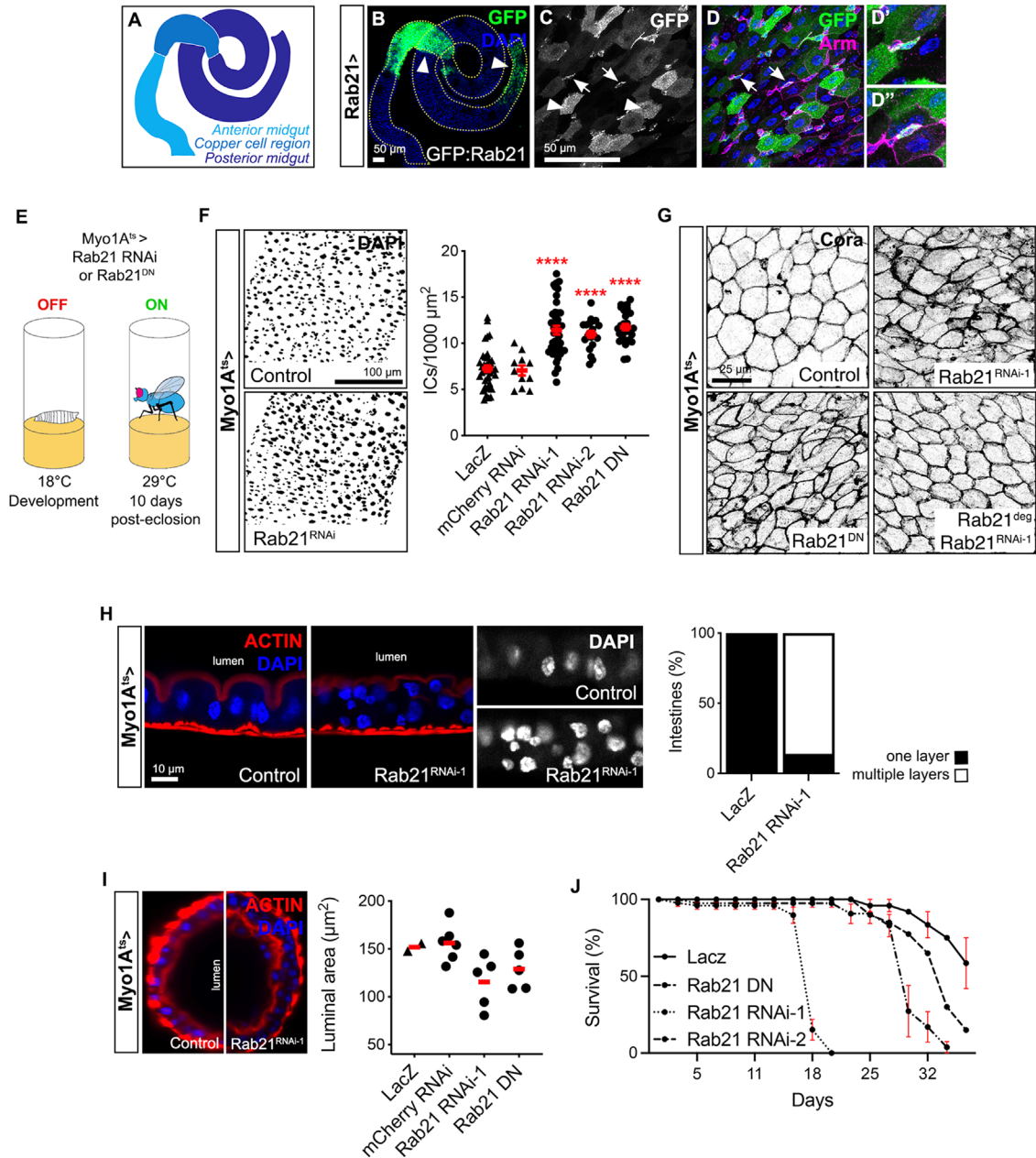
FIGURE 1: Rab21 expression in enterocytes is required to maintain correct intestinal epithelium morphology. (A) Schematic of *Drosophila* midgut compartmentalization. (B–D) Intestine of a *Rab21-GAL4>UAS-GFP:Rab21*[WT] transgenic fly. (B) Arrowheads indicate the copper cell region and the distal posterior midgut and (C) Rab21 enrichment in enterocytes. (D) Arrows show Rab21 enrichment in other Armadillo-positive (Arm[+]) cell types. Images are representative of $n = 15$ guts. (D', D'') Magnifications of the areas highlighted by arrows in D. (E) In adult flies, expression of two independent *Rab21* RNAi hairpins or Rab21[DN] in enterocytes was achieved using Myo1A[ts]-GAL4. (F) Inverted binary images of *Drosophila* guts stained with DAPI and quantification of cell density. (G) Immunostaining for Coracle (Cora). Images are representative of $n = 15–20$ guts. (H) Epithelial organization of guts stained with DAPI and phalloidin. The percentages of guts with single- and multilayered epithelia are shown ($n = 14$ guts). (I) Transverse views of guts stained with DAPI (blue) and phalloidin (red; to detect F-actin) with measurements of luminal areas. (J) Survival curves in controls and flies expressing *Rab21* RNAi or Rab21[DN]. For the LacZ, *Rab21* RNAi-1, and *Rab21* RNAi-2 conditions, $n = 46$, 75, and 47 flies, respectively. For Rab21[DN] $n = 30$ flies. For all experiments $N = 3$, except for I and Rab21[DN] in J, where $N = 2$. ****$P < 0.0001$ by one-way ANOVA followed by Dunnett's test (F).

In various contexts, increased cell density in the intestine is compensated by increased apoptosis (Loudhaief *et al.*, 2017). Hence, we first assessed cell death by immunostaining for cleaved caspase 3. In flies expressing *Rab21* RNAi in enterocytes, the abundance of cleaved caspase 3 was significantly increased compared with controls (Figure 3A). The increased cell death was further corroborated using SYTOX staining (Figure 3B). Consistent with these results, the transcript level of head involution defective (hid), which promotes caspase activity, was up-regulated upon Rab21 depletion (Supplemental Figure 3A).
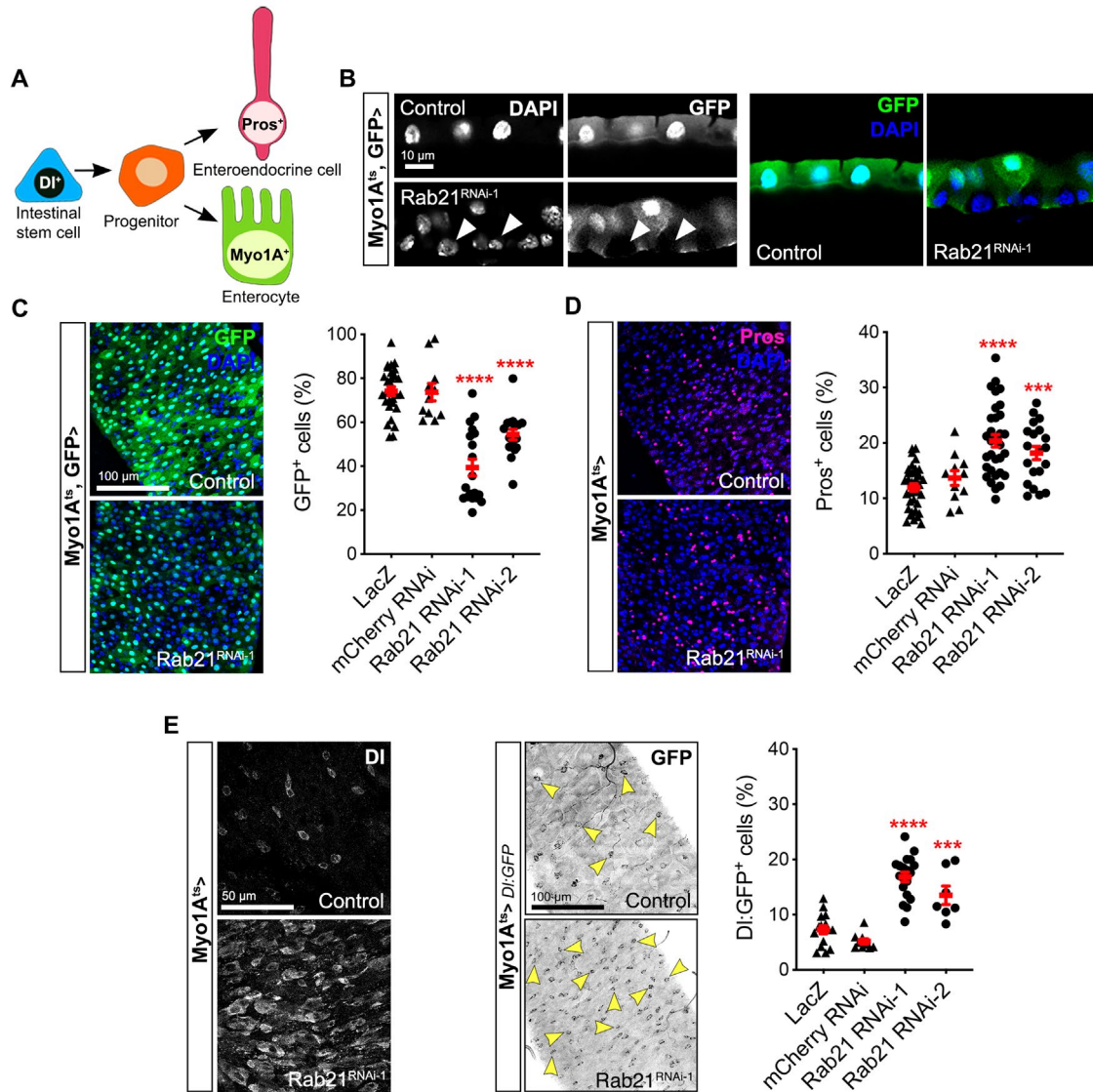
FIGURE 2: Enterocyte Rab21 is required to maintain intestinal homeostasis. (A) Schematic of cell lineages, markers, and GAL4 drivers in the *Drosophila* intestine. (B) GFP was expressed under the control of the enterocyte-specific *Myo1A* promoter to detect enterocytes. Arrowheads indicate accumulating Myo1A⁻ cells. (C) Quantification of the percentage of Myo1A⁺ cells. (D) Immunostaining for Prospero (Pros) and quantification of Pros⁺ cells. (E) Intestinal stem cells were detected using Dl immunostaining or a Dl:GFP reporter. Arrowheads indicate Dl:GFP⁺ cells. Dl:GFP⁺ cells were quantified. ***$P < 0.001$; ****$P < 0.0001$ by one-way ANOVA followed by Dunnett's test (C, D, E). All error bars are the SEM. $N = 3$ for all experiments.

Because cell death in the midgut is often compensated by proliferation (Jiang *et al.*, 2009), we next investigated mitotic activity by immunostaining for histone H3 phosphorylated at serine 10 (pH3). Knockdown of *Rab21* resulted in a significant increase in the percentage of proliferating cells compared with controls (Figure 3C). The pH3⁺ cells were Dl⁺ (Supplemental Figure 3B) and therefore likely intestinal stem cells. Proliferation was also assessed at earlier time points (3 and 5 d); however, we did not observe a common defect in proliferation (Supplemental Figure 3C). Only *Rab21* RNAi-1 showed large increases in the proportion of pH3⁺ cells at 3 and 5 d (Supplemental Figure 3C), consistent with intestinal tissue morphology observations at the same stages (Supplemental Figure 2D). The stronger effect at earlier time points with *Rab21* RNAi-1 could be due to off-target effects; nevertheless, *Rab21* RNAi-related hyperproliferation was significantly reduced upon coexpression of *Rab21* RNAi-1 with Rab21^deg and was completely rescued for *Rab21* RNAi-2

(Figure 3D). This demonstrates that *Rab21* knockdown was responsible for the increased proliferation at 10 d post–RNAi induction.

Upon stress, damaged enterocytes help trigger the compensatory proliferation of intestinal stem cells by secreting the inflammatory cytokine Upd3, which activates JAK-STAT signaling in the intestinal epithelium (Buchon *et al.*, 2009; Jiang *et al.*, 2009). We thus hypothesized that depletion of enterocyte Rab21 leads to non–cell autonomous compensatory proliferation through the Upd3-JAK-STAT signaling axis. Using a Upd3 reporter line, we observed higher levels of the reporter upon Rab21 depletion from enterocytes (Figure 3E; Supplemental Figure 3D). Consistent with this observation, the 10 × STAT92E-GFP reporter revealed a dramatic increase in JAK-STAT signaling activity in intestines expressing *Rab21* RNAi (Figure 3F). These data support the idea that depletion of Rab21 in enterocytes led to increased intestinal proliferation by a non–cell autonomous mechanism.
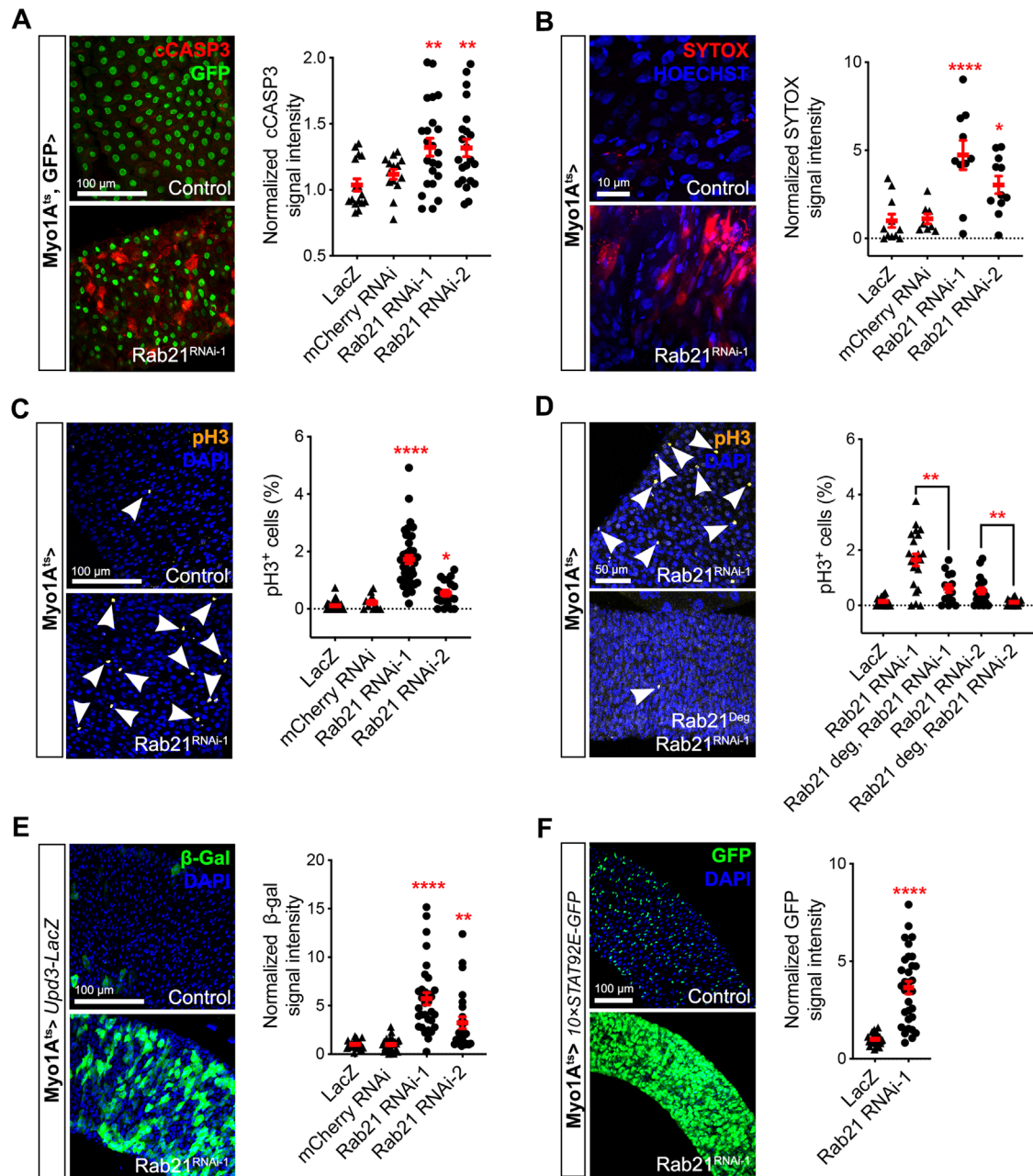
FIGURE 3: Rab21 is necessary for proper cell turnover. (A) Cleaved caspase 3 (cCASP3) immunostaining and (B) SYTOX staining were used to detect apoptotic cells. (A, B) Quantifications of (A) cCASP3 and (B) SYTOX staining intensities. (C, D) Immunostaining for pH3 and quantification of mitotic cell percentages in controls and (C) *Rab21* RNAi alone or (D) *Rab21* RNAi, Rab21[Deg] coexpressing guts. (E) Immunostaining for β-galactosidase (β-Gal) in *Drosophila* intestines expressing a Upd3-LacZ reporter and quantification of β-Gal staining intensities. (F) *Drosophila* guts expressing JAK-STAT activation reporter. Quantification of 10× STAT92-GFP staining intensities. *$P < 0.05$; **$P < 0.01$; ****$P < 0.0001$ by one-way ANOVA followed by Dunnett's test (A, B, C, E), unpaired t test (D), or Mann–Whitney U test (F). All error bars are the SEM. $N = 3$ for all experiments.

Non–cell autonomous proliferation in the Rab21-depleted gut is caused by cell death and activation of the transcriptional coactivator Yki

To confirm that non–cell autonomous proliferation was responsible of the increased numbers of pH3+ cells in intestines with Rab21-depleted enterocytes, we depleted both Upd3 and Rab21 in enterocytes using inducible *upd3* RNAi. Depletion of Upd3 in enterocytes was sufficient to suppress the overproliferation phenotype observed after *Rab21* knockdown (Figure 4A). Enterocyte-derived Upd3 is in-

duced via various pathways in the *Drosophila* adult midgut and, among these, the Hippo and JNK pathways are well documented (Amcheslavsky *et al.*, 2009; Shaw *et al.*, 2010; Houtz *et al.*, 2017; Li *et al.*, 2018; Chen *et al.*, 2020). We performed epistasis experiments using inducible RNAi for *basket* (*bsk*) and *yki* to assess the requirements for the JNK and Hippo pathways, respectively, for increased Upd3 expression upon Rab21 depletion. Only *yki* RNAi expression was sufficient to attenuate the compensatory proliferation induced by Rab21 depletion (Figure 4B). Furthermore, coexpression of
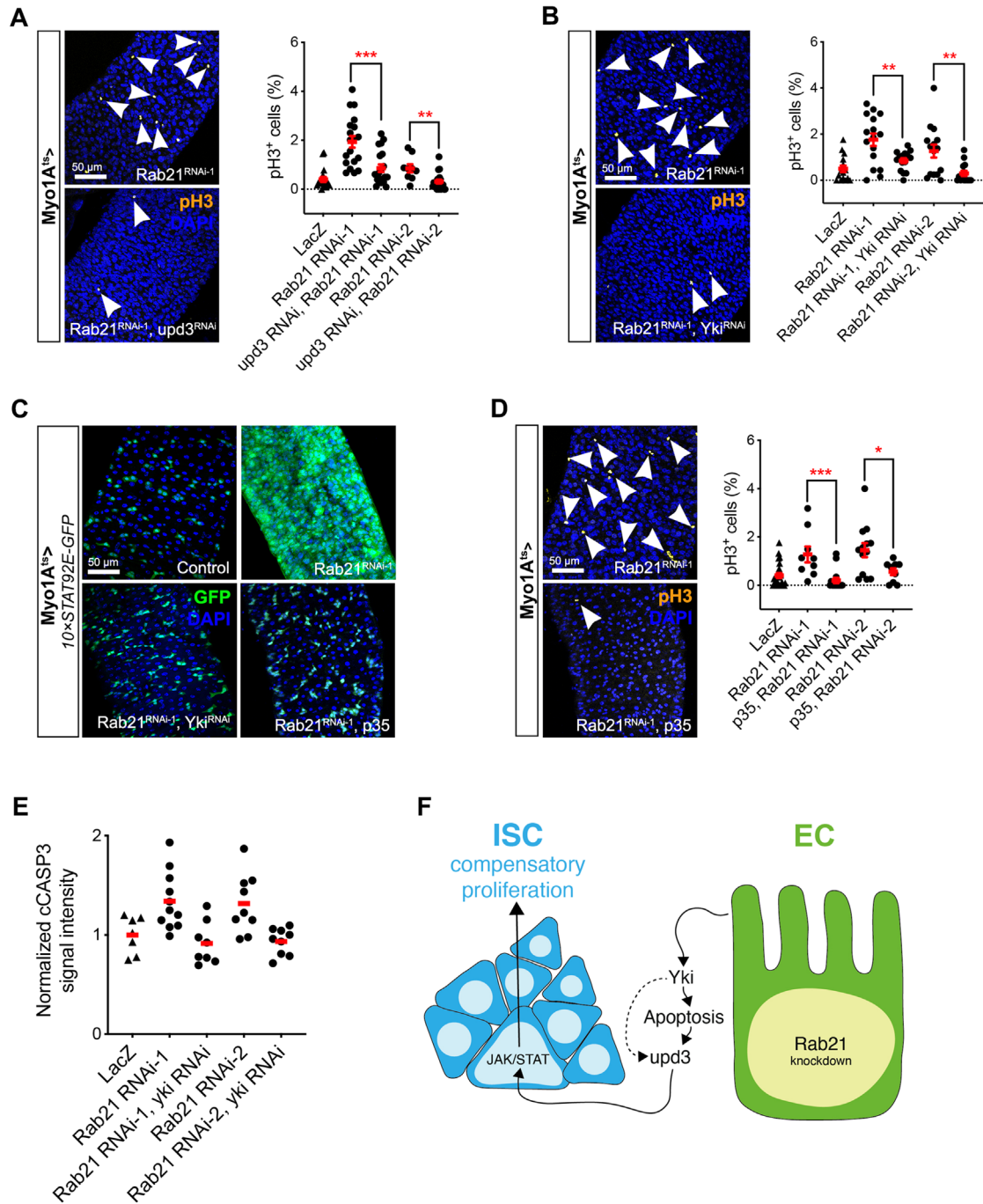
FIGURE 4: Knockdown of *Rab21* affects cell survival in a Yki-dependent manner. (A, B) Immunostaining for pH3 (arrowheads) in fly intestines and quantification of pH3+ cells. (C) Expression of the $10 \times$ STAT92E-GFP reporter in *Drosophila* guts upon *Rab21* knockdown in enterocytes expressing either *yki* RNAi or p35. Images are representative of $n = 16$ guts for p35 overexpression and $n = 10$–15 guts for *yki* knockdown. (D) Immunostaining for pH3 (arrowheads) in fly intestines and quantification of pH3+ cells. (E) Quantifications of cCASP3 staining intensities. (F) Schematic of the signaling pathways affected by Rab21 knockdown in enterocytes (EC) and the indirect consequences on intestinal stem cells (ISC). $*P < 0.05$; $**P < 0.01$; $***P < 0.001$ by unpaired t test (A, B, D, E) or Mann–Whitney U test (A, B, D). All error bars are the SEM. $N = 3$ experiments except for E, where $N = 2$.

Rab21 with *yki* RNAi was sufficient to inhibit JAK/STAT activation (Figure 4C), thus validating Yki's requirement for Upd3 expression upon Rab21 knockdown.

As we observed an increase in the number of apoptotic cells in intestines depleted for Rab21, we also evaluated whether cell death contributes to the increased mitotic activity and Upd3-re-lated inflammatory phenotypes. To do so, we blocked apoptosis by overexpressing the baculovirus antiapoptotic protein p35 in Rab21-depleted enterocytes. In this context, JAK-STAT activation (Figure 4C) and proliferation (Figure 4D) were both largely dimin-ished compared with controls, demonstrating that cell death also increased Upd3 secretion to mediate JAK-STAT activation. We

next investigated whether Yki regulation and apoptosis induction upon Rab21 depletion were related events. Interestingly, cleaved caspase 3 staining was reduced upon co-knockdown of *Rab21* and *yki* in enterocytes (Figure 4E), indicating a link between these events. Dual staining for Upd3 and cleaved caspase 3 upon *Rab21* knockdown revealed that apoptotic cells had low Upd3 levels and were often in proximity to high Upd3–expressing cells (Supplemental Figure 3E). This implies that apoptosis occurs in cells other than those secreting high levels of Upd3. These data show that enterocyte Rab21 is required to block Yki activation and enhance enterocyte survival, both of which participate in restricting intestinal stem cell proliferation in a non–cell autonomous manner (Figure 4F).

Rab21 is required for proper endolysosomal regulation in enterocytes

Rab GTPases are important regulators of cellular trafficking events (Jean and Kiger, 2012), and Rab21 has been associated with diverse trafficking processes, mainly at early endosomes (Pellinen *et al.*, 2006; Yang *et al.*, 2012; Jean *et al.*, 2015; Del Olmo *et al.*, 2019). Therefore, to gain a better understanding of the dysfunctional enterocytic processes causing the physiological responses in the gut, we investigated early endosomal compartments upon Rab21 depletion. Using the GFP:2 × FYVE probe, which labels PtdIns(3)P present at early endosomal membranes, we observed decreased PtdIns(3)P pools in Rab21-depleted enterocytes compared with controls (Supplemental Figure 4A). In addition, immunostaining for the early endosomal marker hepatocyte growth factor regulated tyrosine kinase substrate (Hrs), a well-known PtdIns(3)P-interacting protein (Henne *et al.*, 2011), revealed decreased Hrs$^+$ puncta upon *Rab21* knockdown compared with controls (Supplemental Figure 4B). These data suggest that Rab21 regulates PtdIns(3)P more directly than previously thought (Jean *et al.*, 2012). Our previous work characterizing the Rab21 interactome (Del Olmo *et al.*, 2019) identified close proximity between Rab21 and the phosphatidylinositol-3-phosphate 5-kinase (phosphoinositide kinase, FYVE-type zinc finger containing) that is required to generate phosphatidylinositol-3,5-biphosphate (PtdIns(3,5)P$_2$) from PtdIns(3)P. We therefore also assessed whether the decreased PtdIns(3)P level was due to excessive generation of PtdIns(3,5)P$_2$. Using the mCherry:ML1N2 × probe, which labels PtdIns(3,5)P$_2$, we noticed a significant decrease in PtdIns(3,5)P$_2$ pools in Rab21-depleted intestines compared with controls (Supplemental Figure 4C). PtdIns(3,5)P$_2$ localizes to late endosomal and lysosomal membranes; therefore, we investigated whether these compartments were affected by Rab21 depletion. We noticed a slight increase in Rab7$^+$ vesicles, although there were no significant differences (Supplemental Figure 4D), thus suggesting that late endosomes were not, or only slightly, affected. In addition, we used the GFP-lysosomal–associated membrane protein (LAMP) construct (Pulipparacharuvil, 2005) to assess lysosome localization upon *Rab21* knockdown. As observed in other fly tissues and in mammalian cells (Jean *et al.*, 2015; Del Olmo *et al.*, 2019), we did not notice any differences in the lysosomes of control and enterocytes expressing *Rab21* RNAi (Supplemental Figure 4E). In this context, the formation of intact Rab7$^+$ late endosomes and lysosomes might occur through compensatory routes. Similarly, knockdown of *Rab21* in HeLa cells does not perturb lysosomal formation or function (Jean *et al.*, 2015). These results favor defects in sorting events rather than global failure of the endolysosomal pathway. Altogether, these data show that Rab21 depletion perturbs specific phosphoinositide pools, potentially impacting enterocyte sorting pathways.

Inhibition of autophagy or specific early endosomal regulators phenocopies *Rab21* knockdown in enterocytes

As membrane trafficking and cellular signaling are closely related, the effects of enterocytic Rab21 depletion on endosomal trafficking may impact signaling pathways responsible for the observed phenotypes. To gain deeper insight into the trafficking pathways that regulate enterocyte functions, we performed a genetic screen to identify genes phenocopying the increased compensatory proliferation and inflammation caused by Rab21 depletion by assaying pH3 staining and Upd3 levels, respectively. We focused on endosomal genes linked to different membrane trafficking steps or processes (Figure 5A), as well as genes associated with functions ascribed to Rab21: autophagy regulation (Autophagy-related 4 [*Atg4*], V-associated membrane protein 8 [*Vamp8*], and Syntaxin 17 [*Syx17*]) and Wiskott–Aldrich syndrome protein and Scar homologue (WASH)/ Retromer cargo regulation (washout [*wash*], Strumpellin [*Strump*], family with sequence similarity 21 (*FAM21*), Vacuolar protein sorting (*Vps26*, *Vps29*, and *Vps35*), β1 integrin recycling (*myospheroid* [*mys*]), and EGFR degradation (*Ras^{V12}*). Strikingly, disrupting enterocyte autophagy (*Syx17*, *Vamp8*, *Atg4*, *Atg1*), early endosomal tethering (class C core vacuole/endosome tethering [CORVET] complex genes) (*Vps8*, *Vps18*), and early and late endosomal regulation (*Rab5* and *Rab7*, respectively) led to increased proliferation (Figure 5, B and C) (absolute quantification of pH3$^+$ cells is shown in Supplemental Figure 5A) and Upd3 expression (Figure 5, D and E). As previously characterized (Patel *et al.*, 2015), activated EGFR-MAPK signaling (Ras^{V12}) also led to increased proliferation and Upd3 expression (Figure 5, B–E). Similar results were observed upon expression of a DN form of Shibire (Shi; being the fly orthologue of mammalian Dynamin) (Figure 5, B–E), while depletion of adaptor protein complex 2, α subunit (AP-2), had no effect (Supplemental Figure 5, B and C). Finally, knockdown of the Retromer subunit *Vps26* (Figure 5, B–E) also phenocopied Rab21 depletion; however, depleting two other Retromer subunits (Vps29 and Vps35) did not (Supplemental Figure 5, B and C). None of the other tested genes phenocopied both the overproliferative and inflammatory phenotypes observed upon Rab21 depletion (Supplemental Figure 5, B and C). We conclude that early endosomal functions (Vps26, Rab5, Vps8, and Vps18) and autophagy (Shi, Atg4, Vamp8, and Syx17) are required in enterocytes for intestinal tissue maintenance. Consistent with these findings, a recent study demonstrated that defective autophagy in enterocytes results in increased proliferation and Upd3 levels (Nagai *et al.*, 2021).

A previous study showed that depletion of Rab11 in fly enterocytes results in increased proliferation and Upd3 secretion (Yu *et al.*, 2014). Therefore, we evaluated whether *Rab21* RNAi-related phenotypes could be rescued by increased endosomal recycling, because Rab21 and Rab11 were previously shown to be epistatic (Jean *et al.*, 2012). A constitutively active form of Rab11 was overexpressed in enterocytes depleted of Rab21, and proliferation was assessed. In this context, proliferation was still increased compared with controls and not rescued (Supplemental Figure 5D). This result demonstrates that Rab21 acts independently of Rab11-dependent recycling pathway in enterocytes or that *Rab21* knockdown affects early endosomal compartments to an extent that increased Rab11 activity is not sufficient for rescue.

EGFR signaling is epistatic to Rab21 in enterocytes

Activated Ras phenocopied Rab21 depletion (Figure 5, B–E, and Patel *et al.*, 2015), and interestingly, recent work has highlighted a role for autophagy in the regulation of EGFR-MAPK signaling in *Drosophila* intestinal stem cells (Nie *et al.*, 2019; Du *et al.*, 2020).
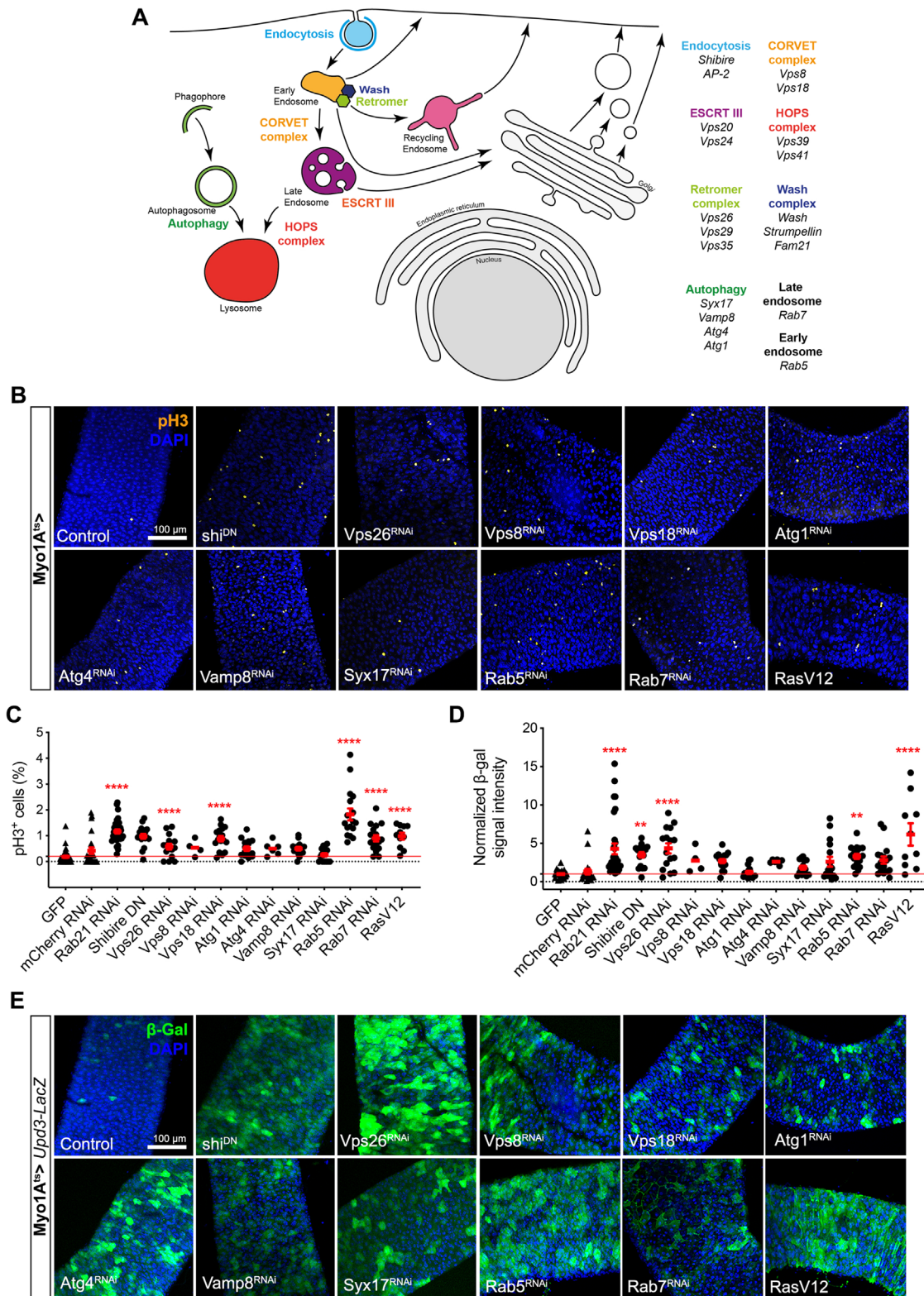
FIGURE 5: Depletion of autophagic genes phenocopies enterocyte *Rab21* knockdown. (A) Subcellular localizations of the genes assessed in the screen. (B) Immunostaining for pH3 after depletion of Vps26, CORVET components, autophagy-related genes, Rab5, or Rab7, or after expression of shi^{DN} or constitutively active Ras. Quantification of (C) pH3$^+$ cells and (D) β-galactosidase signal intensity. (E) Immunostaining for β-galactosidase (β-Gal). *$P < 0.05$; **$P < 0.01$; ****$P < 0.0001$ by one-way ANOVA followed by Dunnett's test (C, D). All error bars are the SEM. $N = 3$ independent experiments, except for *Vps8, Atg4 RNAi*, where $N = 1$.
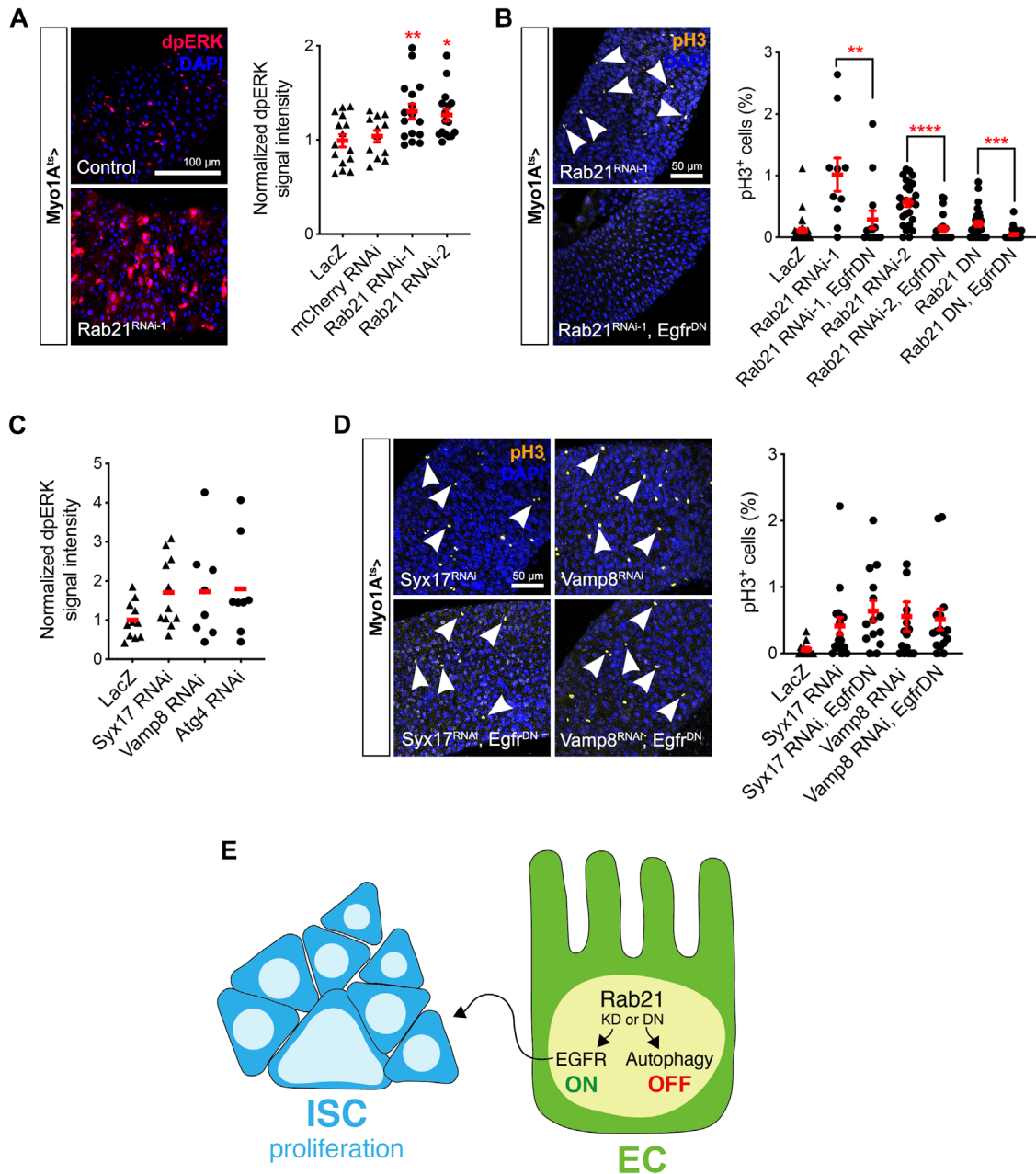
FIGURE 6: Rab21 regulates EGFR signaling in enterocytes independently of autophagy. (A) Immunostaining for dpERK and quantification of dpERK signaling intensity, revealing ERK activation upon Rab21 depletion. (B) Immunostaining for pH3 (arrowheads) in fly intestines coexpressing *Rab21* RNAi in enterocytes with or without Egfr[DN] and quantification of pH3^{+} cells. (C) Quantification of dpERK signal intensity upon depletion of autophagic proteins. (D) Immunostaining of pH3 (arrowheads) upon depletion of autophagic proteins with and without Egfr[DN] overexpression and quantification of pH3^{+} cells. (E) Scheme illustrating how *Rab21* knockdown in enterocytes negatively regulates autophagy independently of EGFR activation-triggered intestinal stem cell proliferation. KD, knockdown. DN, dominant negative. *$P < 0.05$; **$P < 0.01$; ***$P < 0.001$; ****$P < 0.0001$ by one-way ANOVA followed by Dunnett's test (A, C) or Mann–Whitney U test (B, D); ns, nonsignificant. All error bars are the SEM. $N = 3$ independent experiments, except for C, where $N = 2$.

Therefore, we assessed whether EGFR-MAPK signaling was impaired upon *Rab21* knockdown by immunostaining for diphosphorylated extracellular signal–regulated kinase ((dp)ERK). Intestines depleted of Rab21 displayed a significant increase in dpERK compared with controls (Figure 6A). Consistent with EGFR activation, qPCR analysis of the EGFR target genes Mitogen-activated protein kinase phosphatase 3 (*Mkp3*) and *argos* showed that both transcripts were increased upon knockdown of *Rab21* (Supplemental Figure 6A),

although the changes were not statistically significant. Importantly, overexpression of a DN form of Egfr (Egfr[DN]) was sufficient to rescue the non–cell autonomous proliferation of intestinal stem cells induced by *Rab21* RNAi (Figure 6B). These data demonstrate that Rab21 contributes to the regulation of enterocyte EGFR signaling. We next investigated whether this contribution was mediated by regulating autophagy. When we immunostained intestines for Refractory to sigma P (Ref(2)p), an autophagic cargo adaptor, we

noticed an increase in Ref(2)p[+] puncta in Rab21-depleted guts compared with controls (Supplemental Figure 6B). This suggested a deregulation of autophagic flux, as previously observed in other cell types (Jean et al., 2015; Lauzier et al., 2019). These data were further supported by transmission electron microscopy (TEM), which revealed an increased number of autophagosomes, recognizable by their double membranes, upon Rab21 depletion (Supplemental Figure 6C, arrowheads). To validate the involvement of Rab21's autophagic function in the regulation of EGFR signaling, we assessed dpERK signal intensity after depleting autophagy-related genes. Surprisingly, although these knockdowns showed a modest increase in dpERK, no significant differences were observed (Figure 6C; Supplemental Figure 6D). More importantly, expression of dominant negative EGFR was unable to rescue the increased mitotic activity observed in intestines depleted of autophagic genes (Figure 6D). These data show that EGFR signaling and autophagy, respectively, are positively and negatively regulated by Rab21 in enterocytes; however, these effects seem to be independent of each other (Figure 6E). These results also highlight that, unlike in intestinal stem cells, autophagy and EGFR signaling are not epistatic in enterocytes.

Enterocyte *Rab21* knockdown affects solute carrier transporter abundance

The above data identified the cellular signaling pathways affected by Rab21 depletion from enterocytes, based on analysis of candidate genes. However, they do not provide an unbiased view of the proteins affected by *Rab21* knockdown. Therefore, to supplement our genetic analyses, we systematically identified proteins affected by Rab21 depletion in enterocytes. To do so, we performed a TMT-based quantitative proteomic analysis of control fly intestines and those with enterocyte-specific Rab21 depletion in biological triplicate. We identified 2691 proteins in total, of which 101 were differentially modulated more than twofold (Figure 7A), with 57 proteins that increased and 44 that decreased (Figure 7B) in Rab21-depleted cells compared with controls. Interestingly, many of the increased proteins belonged to the solute carrier (SLC) transporter family (Figure 7B, highlighted with a star). Previous studies have demonstrated functional links between Rab21 and certain SLC members (Zhang et al., 2016; Del Olmo et al., 2019), supporting our data. The proteomic approach also revealed decreased levels of several proteins in the cytochrome P450 (CYP) family (Figure 7B, squares), as well as proteins related to proteolysis (Figure 7B, circles). Finally, three proteins related to lipid metabolism were also deregulated upon Rab21 depletion from enterocytes (Figure 7B, hash marks). We then investigated Reactome pathways enriched with differentially regulated proteins (Figure 7C). This analysis revealed the deregulation of several processes related to sugar: "lysosomal oligosaccharide catabolism" was decreased, while "cellular hexose transport," "intestinal hexose absorption," and "glucogenesis" were increased. Consistent with the increase in SLC proteins, "SLC-mediated transmembrane transport" was also enriched. Interestingly, some of the up-regulated SLC proteins are involved in carbohydrate transport, including proteins belonging to the SLC2, SLC5, and SLC16 families. These data led us to conclude that Rab21 is likely required, directly or indirectly, for the proper regulation of specific SLC, CYP, and lipid metabolism proteins and maintains the proper absorption of sugar and potentially other nutrients by enterocytes.

Rab21 in enterocytes is required for Apolpp and Tret1-1 transport

To validate the proteomic data, we investigated the link between Rab21 and two overabundant proteins in Rab21-depleted intestines

linked to lipid and carbohydrate physiology, respectively: Apolipophorin (Apolpp) and Trehalose transporter 1-1 (Tret1-1). Apolpp transports specific lipids, mainly diacylglycerol (DAG), in the hemolymph (Palm et al., 2012). As such, it is mostly involved in lipid transport from enterocytes to organs dedicated to triacylglycerol (TAG) storage (Figure 8A). Immunostaining for Apolpp confirmed its accumulation upon *Rab21* knockdown (Figure 8B), validating the mass spectrometry (MS) results. We observed Apolpp aggregates in some enterocytes, but not in all (Figure 8B, arrowheads). To assess whether lipid transport was impaired upon depletion of Rab21, we analyzed lipid droplets in the intestinal epithelium using Nile Red staining. Interestingly, we found that the number of small lipid droplets was significantly increased upon *Rab21* depletion by RNAi, while the numbers of medium and large lipid droplets were significantly decreased (Figure 8C). Importantly, the total number of lipid droplets appeared diminished after *Rab21* knockdown compared with controls (Figure 8C). These data suggest either less lipid absorption, more lipid transport, or increased lipolysis. We next quantified circulating mono/di/triglycerides in the hemolymph of adult flies; however, we did not detect any differences between control and Rab21-depleted flies (Figure 8D), thus arguing against the excessive lipid transport hypothesis. To further refine these observations, we evaluated lipid droplet morphology in the main TAG storage organ, the fat body (FB). Nile Red staining highlighted an important increase in lipid droplet size and accumulation in fat bodies when Rab21 was depleted from enterocytes compared with controls (Figure 8E), suggesting increased TAG synthesis in the fat body. Because Apolpp is mainly produced by the FB (Palm et al., 2012), and to test whether improper lipid transport could phenocopy Rab21 depletion, we analyzed the impact of *apolpp* knockdown in fat bodies on intestinal tissue morphology and proliferation (Supplemental Figure 7, A and B). Curiously, expression of *apolpp* RNAi did not affect tissue morphology (Supplemental Figure 7A), while it tended to decrease the proliferation rate (Supplemental Figure 7B). Although *apolpp* transcripts are weakly expressed in the gut (Palm et al., 2012), we assessed *apolpp* knockdown in the intestine. Unexpectedly, expression in enterocytes of *apolpp* RNAi dramatically affected lipid droplets in the intestinal epithelium (Supplemental Figure 7C), with small lipid droplets accumulating in enterocytes. Furthermore, immunostaining for Cora and pH3 showed that tissue morphology was impaired (Supplemental Figure 7D), whereas proliferation activity was unchanged (Supplemental Figure 7E). We thus performed an epistasis experiment by simultaneously knocking down *Rab21* and *apolpp* in enterocytes. Neither proliferation nor lipid droplet morphology was rescued in this context (Figure 8, F and G). Altogether these results show the importance of enterocyte Rab21 for correct Apolpp location and lipid droplet size and accumulation in the gut and fat bodies. In addition, we show that Apolpp from the intestine is also required for proper lipid droplet size and accumulation. However, our data demonstrate that the effect of Rab21 on lipid droplets is independent of Apolpp originating from the intestine.

Tret1-1 is a trehalose transporter (Kanamori et al., 2010) (Figure 9A). Trehalose is a carbohydrate that supplies energy to different tissues (e.g., flight muscles and brain) and provides protection in stress condition (Mattila and Hietakangas, 2017). Using transgenic HA-tagged *Tret1-1* flies (Volkenhoff et al., 2015) we validated that Tret1-1 levels were increased upon Rab21 depletion in enterocytes (Figure 9B). As observed for Apolpp, Tret1-1 accumulation was restricted to a subset of enterocytes (Figure 9B, arrowheads). We first investigated whether *Tret1-1* knockdown would impair intestinal tissue. Cell junction staining for Cora showed that Tret1-1
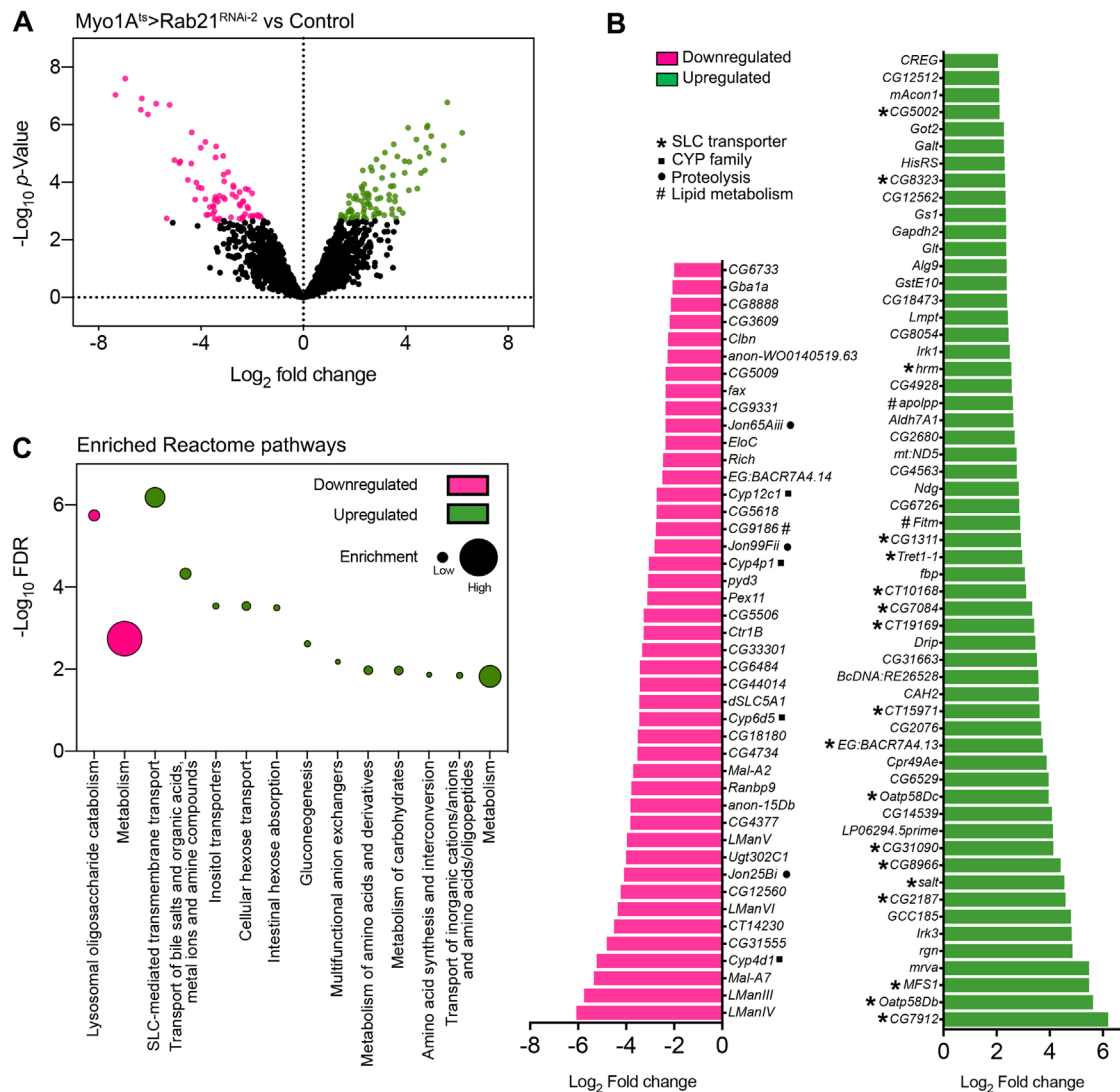
FIGURE 7: TMT-based quantitative proteomic analysis of Rab21-depleted guts. (A) Volcano plot of protein abundance differences between Myo1A[ts]>$Rab21$[RNAi-2] and control guts in N = 3 independent biological replicates. Pink indicates an FDR < 0.05 and a $\log_2$ fold change (FC) < 1.5; while green indicates an FDR < 0.05 and a $\log_2$ FC > 1.5. (B) Genes associated with proteins with significant (FDR < 0.05) decreases (pink) or increases (green) in abundance ($\log_2$ FC of < 2 and > 2, respectively), with their associated FCs. (C) Reactome pathways enriched with proteins with significantly (FDR < 0.05) decreased (pink) or increased abundance ($\log_2$ FCs of < –2 and > 2, respectively). The distance of each circle from the horizontal axis represents the –$\log_{10}$ FDR of that pathway. The diameter of each circle corresponds to the number of proteins with modified abundance in that specific pathway compared with the total number of proteins with modified abundance.

depletion affected tissue morphology (Figure 9C). However, quantification of pH3[+] did not highlight any changes in the proportion of mitotic cells compared with controls (Figure 9D). On the basis of Tret1-1's function, we next assessed circulating levels of trehalose and glucose in the hemolymph of adult flies depleted of Rab21 (Figure 9E). Interestingly, although the results were not significantly different, trehalose and glucose amounts tended to be decreased upon $Rab21$ RNAi expression compared with controls (Figure 9E). Finally, co-knockdown of $Rab21$ and $Tret1-1$ did not abolish $Rab21$ RNAi-related hyperproliferation (Figure 9F). These data show that Rab21 regulates the Tret1-1 levels and, consequently, indirectly affects circulating sugar levels. Independently of Rab21, our results also suggest that Tret1-1 is important for maintaining proper tissue morphology.

DISCUSSION

The importance of membrane trafficking machinery in cell homeostasis is well established (Yarwood *et al.*, 2020); however, questions remain regarding the cell type–specific functions of the majority of its components. In enterocytes, previous studies uncovered a role for endosomal recycling in coordinating apical-basal axis formation (Sato *et al.*, 2007; Knowles *et al.*, 2015; Nie *et al.*, 2019) and brush border formation. Here, we found that the early endosomal protein Rab21 is required in enterocytes to maintain tissue equilibrium by regulating multiple signaling events.

Rab21 depletion affects intestinal tissue organization

We showed that $Rab21$ knockdown in enterocytes leads to the formation of a multilayered epithelium with aberrant localization of
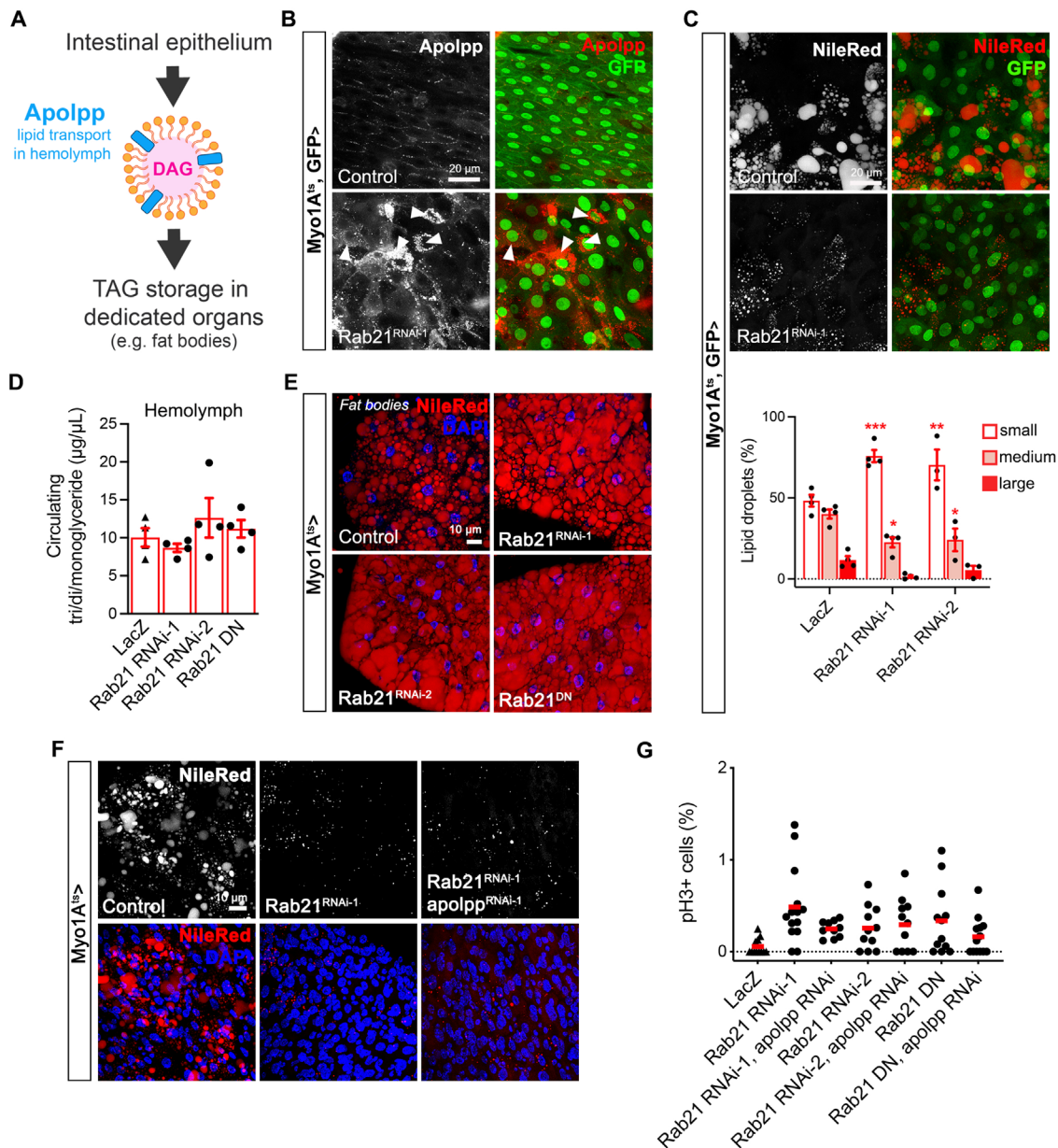
FIGURE 8: Enterocyte Rab21 influences intestinal and fat body lipid droplets. (A) Apolpp is required for diglyceride (DAG) transport. (B) Immunostaining for Apolpp. Images are representative of $n = 15$ images. (C) Nile Red staining and quantification of lipid droplet sizes in intestines from controls and *Rab21* RNAi-expressing flies. $n = 20–30$ guts. (D) Quantification of circulating tri/di-monoglycerides in the hemolymph. (E) Nile Red staining in fat bodies from controls and flies depleted for Rab21. $n = 15–25$ fat bodies. (F) Nile Red staining and (G) quantification of pH3^{+} cells in fly intestines codepleted of Rab21 and Apolpp. Images are representative of 15–20 guts. $*P < 0.05$; $**P < 0.01$; $***P < 0.001$ by one-way ANOVA followed by Dunnett's test (D), two-way ANOVA followed by Dunnett's test (C), or Mann–Whitney U test (G). All error bars are the SEM. $N = 5$ independent experiments for E, $N = 4$ for C, D, and F, $N = 3$ for B, and $N = 2$ for G.

the adherens and septate junction markers Arm and Cora. Intriguingly, while flies depleted of enterocyte Rab21 have shorter lifespans, epithelium integrity is conserved, indicating that the reduced lifespan is not due to tissue leakiness. Similarly, flies depleted of intestinal septate and adherens junction components (tetraspanin 2A and E-cadherin, respectively) do not show tissue permeability defects (Zhao *et al.*, 2018; Xu *et al.*, 2019). Therefore, Cora and Arm mislocalization in Rab21-depleted guts may reflect defects in maintenance of tissue organization and related signaling events rather than impaired junction formation and function.

Our data illustrate that intestinal cell equilibrium is dramatically perturbed upon Rab21 depletion from enterocytes. The enterocyte population diminished while the intestinal stem cell and enteroendocrine cell populations expanded. This expansion in the numbers of intestinal stem cells and enteroendocrine cells could account for the increased cellular density. Our results indicate that the reduction in enterocytes is due to induction of apoptosis and that compensatory proliferation is responsible for the rise in intestinal stem cells. Interestingly, previous studies in humans and mice showed that Rab21 levels are low in the crypts of the small intestine and high in villi
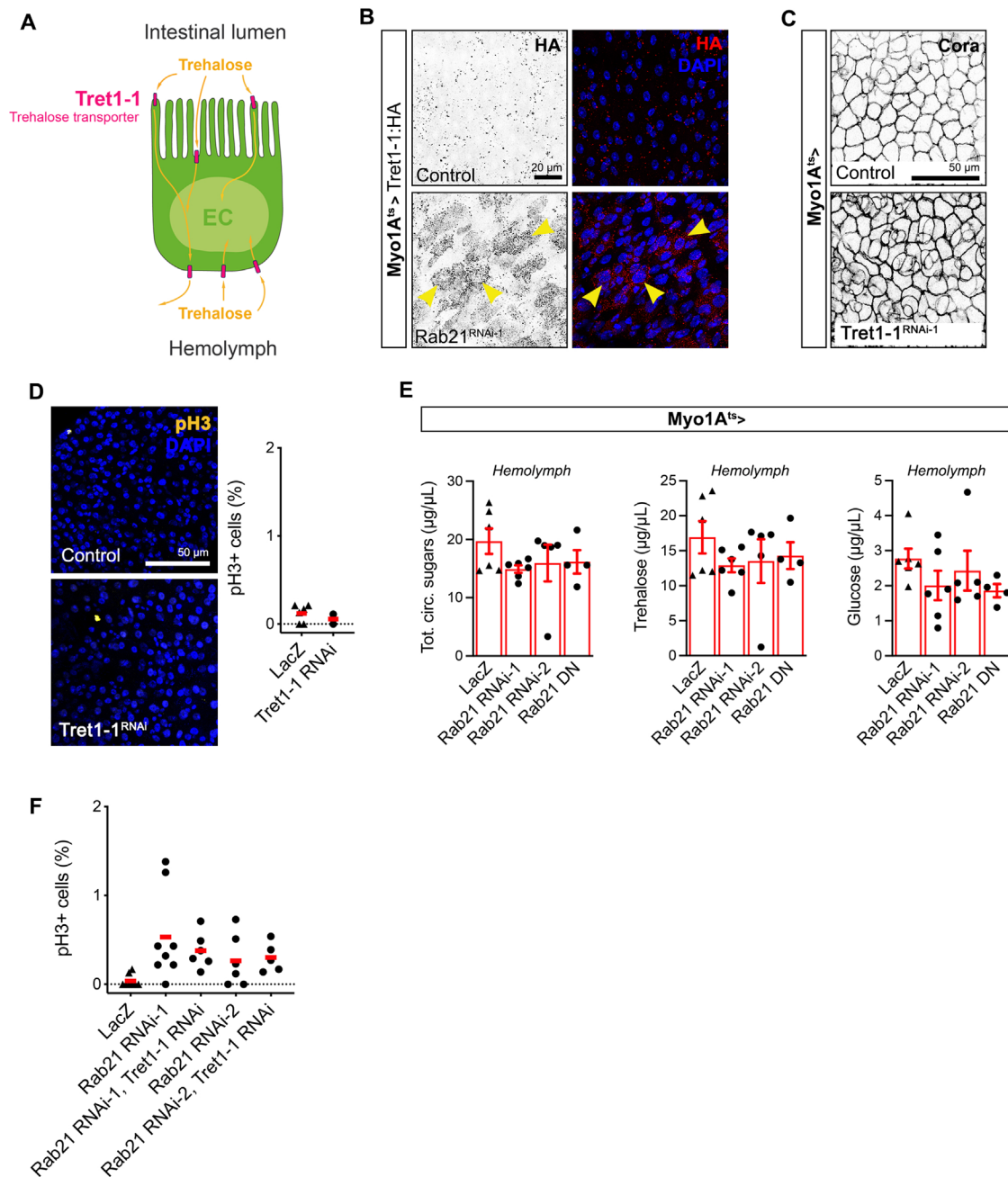
FIGURE 9: The trehalose transporter Tret1-1 accumulates upon Rab21 depletion from enterocytes. (A) Scheme illustrating Tret1-1's trehalose transport function. (B) Control and Rab21-depleted guts from Tret1-1:HA flies were immunostained for HA. Images are representative of $n = 15$ guts. (C, D) Guts were immunostained for Cora (C) or pH3 (D). Images are representative of two to six guts. (E) Quantification of trehalose and glucose levels in the hemolymph of control and Rab21-depleted guts. (F) Quantification of pH3+ cells in fly intestines codepleted of Rab21 and Tret1-1 were stained for pH3. Unpaired t tests (D, F) or one-way ANOVA followed by Dunnett's test (E) were used for statistical analysis. All error bars are the SEM. $N = 4$ independent experiments for E, $N = 3$ for B, and $N = 1$ for C, D, and F.

epithelial cells (Opdam *et al.*, 2000; Zhang *et al.*, 2016), suggesting that Rab21 importance for enterocyte functions is likely conserved.

Rab21 knockdown is epistatic to multiple pathways

It is unclear why we observed expansion of the enteroendocrine cell population. Previous studies highlighted a role for the JAK-STAT pathway in enteroendocrine cell specification (Beebe *et al.*, 2010; Lin *et al.*, 2010). A high level of JAK-STAT signaling is required for enteroendocrine fate specification, demonstrated by

the fact that the intestinal epithelia of hypomorphic *Stat92*[E06346] mutant flies are composed mainly of enterocytes (Lin *et al.*, 2010). Interestingly, we showed that intestines depleted of Rab21 display a massive increase in JAK-STAT signaling activity. Therefore, it is conceivable that the increase in enteroendocrine cells is caused by hyperactivation of the JAK-STAT pathway in progenitor cells.

In addition, we observed the induction of inflammation upon Rab21 depletion. This inflammation was mediated by Upd3 secretion and led to compensatory proliferation. Enterocytes secrete

inflammatory cytokines in response to a large range of stresses (e.g., apoptosis, infection, reactive oxygen species, JNK activation, injury) (Amcheslavsky et al., 2009; Jiang et al., 2009, 2011; Ren et al., 2010; Shaw et al., 2010; Staley and Irvine, 2010; Patel et al., 2019), with Upd3 being the most abundant (Jiang et al., 2009). Secretion of Upd3 triggers compensatory proliferation by activating JAK-STAT signaling in intestinal stem cells and visceral muscle cells (Jiang et al., 2009; Lin et al., 2010). Visceral muscle cells, in turn, secrete the Egfr ligand Vein, which promotes intestinal stem cell proliferation through Egfr (Buchon et al., 2010; Jiang et al., 2011). Various signaling pathways act as stress sensors in the intestinal epithelium, including the Hippo-Yki, JNK, and p38 pathways (Amcheslavsky et al., 2009; Ren et al., 2010; Shaw et al., 2010; Staley and Irvine, 2010; Patel et al., 2019).

In enterocytes, activation of any one of these pathways stimulates Upd3 secretion (Jiang et al., 2009; Ren et al., 2010; Shaw et al., 2010; Staley and Irvine, 2010; Patel et al., 2019). Interestingly, constitutive activation of the JNK pathway induces cell death (Jiang et al., 2009). However, enterocyte apoptosis is not responsible for JNK-mediated compensatory proliferation, because JNK-induced compensatory proliferation cannot be rescued by p35 expression (Jiang et al., 2009). In addition to Upd3 secretion, stressed enterocytes promote intestinal stem cell proliferation through transcriptional activation of the Egfr ligand maturation factor Rhomboid, which promotes secretion of mitogenic Egfr ligands (Liang et al., 2017). Consistent with these data, in Rab21-depleted guts, inhibiting JNK signaling did not rescue the compensatory proliferation, whereas blocking apoptosis significantly reduced it. Furthermore, we showed that Yki was required for compensatory proliferation of intestinal stem cells, as well as for apoptosis activation, after Rab21 depletion. The Hippo-Yki pathway plays well-characterized roles in promoting cell growth/proliferation and inhibiting cell death (Misra and Irvine, 2018); therefore, how Yki signaling and apoptotic signaling combine to trigger compensatory proliferation in Rab21-depleted intestines remains unclear. We observed that the enterocytes expressing high levels of Upd3 were distinct from the dying enterocytes. It is likely that the Yki and apoptosis pathways act synergistically in different enterocytes, both being required to mediate the non–cell autonomous proliferation of intestinal stem cells upon Rab21 knockdown, and may not be individually sufficient for this purpose. Because we could abolish apoptosis by codepleting Yki with Rab21 in enterocytes, and because Yki is mostly involved in cell growth and cell survival, we hypothesize that Yki could enhance the survival of Rab21-depleted cells and trigger apoptosis of neighboring cells. This process has been recently described in the fly gut, where tumor growth caused cell delamination and apoptosis in healthy neighboring enterocytes by affecting their tension forces, culminating in increased Upd3 secretion that fueled tumor growth (Zhou et al., 2021). Moreover, a recent study showed that in unchallenged conditions, Yki depletion from enterocytes tended to diminish enterocyte apoptosis, while Hippo inhibition tended to increase it (Loudhaief et al., 2017). Such data suggest context-dependent requirements for Yki functions, with the Hippo-Yki pathway involved in enterocyte apoptosis in normal conditions. These examples support the hypothesis that Rab21 knockdown, in the subset of enterocytes expressing it, may trigger apoptosis in a non–cell autonomous manner in healthy neighboring cells, via a cell competition mechanism mediated through Yki activation.

The compensatory proliferation and inflammation phenotypes associated with Rab21 depletion from enterocytes are similar to those observed in Rab11-depleted fly intestines (D'Agostino et al., 2019; Nie et al., 2019). However, these phenotypes are related to distinct signaling dysfunctions. We showed that in enterocytes, Rab21 negatively regulates EGFR signaling, while Rab11 functions independently of this pathway (D'Agostino et al., 2019; Nie et al., 2019). Furthermore, we showed that constitutively activated Rab11 does not abolish the overproliferation induced by RNAi-mediated Rab21 depletion in enterocytes. Overexpression of Egfr^DN in Rab21-depleted guts suppressed compensatory proliferation. Consistent with these findings, in HeLa and HEK293T cells, Rab21 is required for proper EGFR internalization and degradation (Yang et al., 2012), although the specific molecular mechanism by which it regulates EGFR remains to be defined. Our genetic screen revealed that depletion of autophagy- and endosome-linked genes from enterocytes phenocopied knockdown of Rab21. Furthermore, constitutive activation of EGFR-MAPK signaling via Ras^V12 expression led to similar results, as previously observed (Patel et al., 2015). Recently, an autophagy–endocytosis network was linked to negative regulation of EGFR signaling in intestinal stem cells (Zhang et al., 2019; Du et al., 2020). However, EGFR pathway regulation appears to be different in enterocytes, as inhibiting EGFR signaling did not rescue autophagy-induced increases in proliferation. Therefore, our data show that autophagy and EGFR signaling are independent in enterocytes, although they are both regulated by the early endosomal protein Rab21.

Proteomic analysis identifies two independent physiological processes affected by Rab21 knockdown

The elevated levels of multiple SLC families observed by TMT-based quantitative proteomic analysis are consistent with previously reported roles for Rab21 (Del Olmo et al., 2019; Moreno-Layseca et al., 2021) and suggest that SLC transporters accumulate either intracellularly or at the plasma membrane in Rab21 knockdown enterocytes. Rab21 has recently been reported to be involved in clathrin- and dynamin-independent endocytosis (Del Olmo et al., 2019; Moreno-Layseca et al., 2021). Thus, both scenarios are consistent with Rab21's functions. However, we favor the possibility that SLCs accumulate in intracellular vesicles that are improperly targeted for degradation, or that they are not recycled efficiently to the plasma membrane and are present in aberrant/inefficient recycling endosomes, given that Rab21 depletion sensitizes enterocytes to cell death. We speculate that the opposite would occur in conditions where more transporters would be at the cell surface. Consistent with this hypothesis, we validated increased levels of the trehalose transporter Tret1-1 upon Rab21 silencing. Trehalose, a disaccharide made of two glucose units, is the most abundant carbohydrate in the hemolymph of insects. It supplies energy to different tissues (e.g., the flight muscles and brain) and provides protection in stress conditions (Mattila and Hietakangas, 2017). Tret1-1 allows trehalose secretion from fat bodies, where it is synthetized, and mediates trehalose uptake in other tissues (Kanamori et al., 2010). Circulating trehalose and glucose levels slightly decreased upon Rab21 knockdown (Figure 9E), suggesting that Tret1-1 accumulates at an improper location in enterocytes. Interestingly, upon Tret1-1 depletion from enterocytes, we observed damaged intestinal tissue morphology. This result indicates the importance of proper trehalose levels in epithelial cells and a role for Rab21 in regulating Tret-1 localization. In our imaging experiments, Tret1-1 did not show apico–basal polarity; thus, it will be interesting to test in future studies whether Rab21 depletion has general effects on transmembrane transporters or targets mainly apically or basally localized cargoes.

Lipoproteins are crucial actors in lipid transport, and changes in their levels are associated with metabolic diseases such as obesity (Eckel et al., 2005). Our data highlight the accumulation of Drosophila apolipoprotein Apolpp in the guts of Rab21-depleted flies. DAG

export from enterocytes is achieved by Apolpp, which then transports them to different storage organs (Palm *et al.*, 2012). Upon knockdown of *Rab21*, lipid droplet content was affected in both the intestine and the fat body, which demonstrates an important function for Rab21 in lipid droplet transport or metabolism, although its exact roles remain to be defined. Consistent with an intestinal role for Rab21 in lipid metabolism, recent studies identified genetic variants for *Rab21* associated with abnormal body mass indexes and increased high density lipoprotein levels (Turcot *et al.*, 2018; Carlson *et al.*, 2021). From our results, and the single nucleotide polymorphisms (SNPs) observed in patients with obesity (Turcot *et al.*, 2018; Carlson *et al.*, 2021), we posit that intestinal Rab21 affects lipid metabolism and mobilization in the intestine. Further investigation of the effects of *Rab21* variants on lipid transport or uptake in *Drosophila* will contribute to the molecular understanding of *Rab21* SNPs in humans.

Our data also reveal decreases in several proteins related to proteolysis. These are likely digestive enzymes mostly produced by enterocytes that are responsible for breaking down ingested macromolecules before their absorption (Engevik and Goldenring, 2018). Decreased digestive enzymes might result in improper absorption, leading to nutrient deprivation that could ultimately reduce lifespan. Untangling these observations will be of great interest in future studies.

To conclude, our data shed light on the importance of the enterocyte early endosomal machinery in maintaining proper tissue equilibrium in the intestines. Our results demonstrate that in enterocytes, Rab21 acts in a manner different from that of Rabs previously investigated in this cell type. We show that Rab21 regulates the EGFR pathway and autophagy, although independently of each other. Moreover, we identify the deregulation of Apolpp and Tret1-1, indicating physiological defects in enterocyte-specific processes related to lipids and carbohydrates. Further studies of the cell-specific functions of membrane trafficking regulators will highlight their underappreciated roles in tissue and organismal homeostasis.

MATERIALS AND METHODS
Request a protocol through *Bio-protocol*.

Drosophila strains
Fly stocks were maintained at 25°C on a standard diet composed of 7 g/l agar, 60 g/l cornmeal, 60 g/l molasses, 23.5 g/l yeast extract, 4.5 ml/l Tegosept (BioShop), and 4 ml/l propionic acid. Genotypes used in this study were 1) *w1118* (VDRC_60000), 2) *y1, w*, Rab21-GAL4* (BDSC_51593), 3) *w1118; UAS-GFP:Rab21 WT* (Jean *et al.*, 2012), 4) *w1118; UAS-GFP:Rab21T27N DN* (Jean *et al.*, 2012), 5) *w1118; UAS-GFP:Rab21Q73L CA* (Jean *et al.*, 2012), 6) *Myo1A-GAL4; Tub-GAL80ts, UAS-GFP* (Jiang *et al.*, 2009), 7) *w1118; P{w[+mC] = UAS-lacZ.B}Bg4-1-2* (BDSC_1776), 8) *y1, sc*, v1; P{y[+t7.7] v[+t1.8] UASt-RNAi mCherry}attP2* (BDSC_35785), 9) *UAS-Rab21 RNAi-1* (VDRC_32941), 10) *w1118; UAS-Rab21 RNAi-2* (VDRC_109991), 11) *y1, w*; Mi{PT-GFSTF.1}Dl[MI04868-GFSTF.1]/TM6C, Sb1 Tb1* (BDSC_59819, Dl:eGFP), 12) *Myo1A-GAL4, Tub-GAL80ts; upd3-LacZ* (Jiang *et al.*, 2011), 13) *w1118; P{w[+mC] = 10XStat92E-GFP}1* (BDSC_26197), 14) *w*; P{w[+mC] = UAS-p35.H}BH2* (BDSC_5073), 15) *y1, sc*, v1, sev21; P{y[+t7.7] v[+t1.8] = TRiP.HMS00646}attP2* (BDSC_32859, *upd3* RNAi), 16) *y1, v1; P{y[+t7.7] v[+t1.8] = TRiP.HMS00041}attP2* (BDSC_34067, *yki* RNAi), 17) *w1118; UAS-GFP:2 × FYVE* (Wucherpfennig *et al.*, 2003), 18) *w1118; UAS-mCherry:ML1N2 x*, 19) *y1, v1; P{y[+t7.7] v[+t1.8] = TRiP.JF02819}attP2* (BDSC_27735, *mys* RNAi), 20) *y1, w*; P{w[+mC] = UAS-shi.K44A}4-1; P{w[+mC] = UAS-shi.K44A}3-7* (BDSC_5811, shiK44A DN), 21) *y1, v1; P{y[+t7.7]*

v[+t1.8] = TRiP.HMS01769}attP40 (BDSC_38937, *Vps26* RNAi), 22) *w1118; UAS-Vps8 RNAi* (VDRC_105952), 23) *y1, sc*, v1, sev21; P{y[+t7.7] v[+t1.8] = TRiP.HMS03720}attP40* (BDSC_54460, *Vps18* RNAi), 24) *y1, sc*, v1, sev21; P{y[+t7.7] v[+t1.8] = TRiP.HMS01482}attP2* (BDSC_35740, *Atg4* RNAi), 25) *UAS-Vamp8 RNAi* (NIG-FLY_1599R-1), 26) *y1, v1; P{y[+t7.7] v[+t1.8] = TRiP.JF01937}attP2* (BDSC_25896, *Syx17* RNAi), 27) *y1, v1; P{y[+t7.7] v[+t1.8] = TRiP.JF02273}attP2* (BDSC_26731, *Atg1* RNAi), 28) *w1118, UAS-Rab5 RNAi* (VDRC_34096), 29) *w1118, UAS-Rab7 RNAi* (VDRC_40337), 30) *w*; P{w[+mC] = UAS-Ras85D.V12}2* (BDSC_64196, *RasV12*), 31) *y1, sc*, v1, sev21; P{y[+t7.7] v[+t1.8] = TRiP.HMS00653}attP2* (BDSC_32866, *AP-2* RNAi), 32) *y1, w*; P{w[+mC] = UAS-Egfr.DN.B}29-77-1; P{w[+mC] = UAS-Egfr.DN.B}29-8-1* (BDSC_5364, EgfrDN), 33) *y1, sc*, v1; P{y[+t7.7] v[+t1.8] = TRiP.HMC05339}attP40* (BDSC_62866, *wash* RNAi), 34) *y1, sc*, v1, sev21; P{y[+t7.7] v[+t1.8] = TRiP.HMC03481}attP40* (BDSC_51906, *Strump* RNAi), 35) *y1, sc*, v1; P{y[+t7.7] v[+t1.8] = TRiP.GLC01693}attP2* (BDSC_50571, *FAM21* RNAi), 36) *UAS-Vps35 RNAi* (VDRC_45570), 37) *w1118; UAS-Vps39 RNAi* (VDRC_40427), 38) *y1, sc*, v1; P{y[+t7.7] v[+t1.8] = TRiP.HMJ21316}attP2* (BDSC_53951, *Vps29* RNAi), 39) *y1, v1; P{y[+t7.7] v[+t1.8] = TRiP.HMS02142}attP40* (BDSC_40894, *Vps20* RNAi), 40) *y1, v1; P{y[+t7.7] v[+t1.8] = TRiP.HMS01733}attP40* (BDSC_38281, *Vps24* RNAi), 41) *y1, v1; P{y[+t7.7] v[+t1.8] = TRiP.HMS00190}attP40* (BDSC_34871, *Vps41* RNAi), 42) *y1, v1; P{y[+t7.7] v[+t1.8] = TRiP.HM05157}attP2* (BDSC_28946, *apolpp* RNAi), 43) *y1, sc*, v1, sev21; P{y[+t7.7] v[+t1.8] = TRiP.HMS02573}attP2* (BDSC_42880, *Tret1-1* RNAi), and 44) *y1, w*; P{w[+mC] = UASpYFP.Rab11.Q70L}* (BDSC_9791, YFP:Rab11Q70L).

New genotypes generated in this study were 1) *w1118; UAS-Rab-21deg/ TM3, Sb, Ser*, 2) *w1118; Myo1A-GAL4, Tub-GAL80ts; UAS-Rab-21deg/ TM3, Ser*, 3) *w1118; Myo1A-GAL4, Tub-GAL80ts; Dl:eGFP/ TM3, Ser*, 4) *w1118; UAS-Rab21 RNAi-1, 10 × STAT92E-GFP*, 5) *w1118; 10 × STAT92E-GFP; UAS-LacZ*, 6) *w1118; Myo1A-GAL4, Tub-GAL80ts; UAS-P35*, 7) *w1118; Myo1A-GAL4, Tub-GAL80ts; UAS-upd3 RNAi*, 8) *w1118; Myo1A-GAL4, Tub-GAL80ts; UAS-yki RNAi*, 9) *w1118; Myo1A-GAL4, Tub-GAL80ts; UAS-EgfrDN*, 10) *w1118; Myo1A-GAL4, Tub-GAL80ts; UAS-mCherry:ML1N2 x*, 11) *w1118; Myo1A-GAL4, Tub-GAL80ts; UAS-GFP:2 × FYVE*, 12) *w1118; Myo1A-GAL4, Tub-GAL80ts; UAS-apolpp RNAi*, 13) *w1118; Myo1A-GAL4, Tub-GAL80ts; UAS-Tret1-1 RNAi*, and 14) *w1118; Myo1A-GAL4, Tub-GAL80ts; UAS-YFP:Rab11Q70L*.

The following genotypes were used as controls: 1) *w1118; P{w[+mC] = UAS-lacZ.B}Bg4-1-2* (BDSC_1776), 2) *y1, sc*, v1; P{y[+t7.7] v[+t1.8] UASt-RNAi mCherry}attP2* (BDSC_35785), and 3) *y* w*; P{w[+mC] = UAS-2xEGFP}AH2* (Alan Michelson, Brigham and Women's Hospital, Boston, USA).

Generation of the UAS-Rab21deg transgenic line
The *Drosophila* Rab21 coding sequence was modified to prevent knockdown of transgene expression without affecting the Rab21 amino acid sequence by mutating the third nucleotide of each codon present in the sequences targeted by *Rab21* RNAi-1 and -2. The *Rab21 degenerate* coding sequence was synthetized by Integrated DNA Technology and cloned into the pUASt-attB plasmid to generate pUASt-dRab21deg. Transgenic flies were generated by Genome Prolab through phiC31 transgenesis at the attP2 landing site. The nucleotide sequence for the degenerate *Rab21* is provided in Supplemental Figure 8.

Immunofluorescence
Drosophila intestines were dissected in 1 × phosphate-buffered saline (PBS) for 20 min, fixed for 2 h in 4% paraformaldehyde at room

temperature (RT), and rinsed three times in PBS. To allow food to exit the lumen, the guts were trimmed and incubated for 20 min in 50% glycerol/PBS and 10 min in PBS–0.1% Triton X-100 (PBT). Intestines were then blocked for 1 h in 20% goat serum/PBT and processed for immunostaining. Primary antibody incubations were performed overnight at 4°C in PBT. The following primary antibodies were used: mouse anti-Cora (C566.9; Developmental Studies Hybridoma Bank [DSHB], Iowa City, IA; 1/100), mouse anti-Arm (N2 7A1; DSHB; 1/100), mouse anti-Pros (MR1A; DSHB; 1/100), mouse anti-Dl (C594.9B; DSHB; 1/100), mouse anti–β-galactosidase (Promega #Z3781; 1/500), rabbit anti-pH3 (Ser10; #06-570; Millipore, Oakville, ON, Canada; 1/1000), rabbit anti–cleaved caspase 3 (#9661; Cell Signaling Technology, Danvers, MA; 1/500), rabbit anti-Ref(2)p (ab178440; Abcam; 1/500), rabbit anti-dpERK (Thr202/Tyr204; #4370; Cell Signaling Technology; 1/500), and mouse anti-Hrs (Hrs 27-4; DSHB; 1/100). Fluorescent secondary antibody incubation was performed for 2 h at RT in PBT. The following secondary antibodies were used (all from Thermo Fisher Scientific): anti-mouse Alexa Fluor 546 (#A11003; 1/500), anti-mouse Alexa Fluor 488 (#A11029; 1/500), anti-rabbit Alexa Fluor 546 (#A11035; 1/500), and anti-rabbit Alexa Fluor 488 (#A11008; 1/500). Phalloidin-Alexa Fluor 546 (#A22283; Thermo Fisher Scientific; 1/500) staining was performed at the same time as secondary antibody incubation. Tissues were mounted in SlowFade Gold Antifade Mountant with DAPI (#S36938; Thermo Fisher Scientific).

In situ hybridization

Day 1: Intestines were fixed in 4% formaldehyde for 45 min at RT, rinsed three times in PBT, and dehydrated using an ethanol gradient in PBT (25%, 50%, 75%, and 100% ethanol for 5 min each at RT). Before hybridization, tissues were successively rehydrated in 50% methanol/PBT and PBT for 10 min each at RT. Intestines were transferred to 50% hybridization buffer (HB; 50% deionized formamide, 5× saline sodium citrate [SSC], 0.1% Triton X-100, 2 mM vanadyl ribonucleoside, 100 µg/ml sonicated salmon sperm DNA, 100 µg/ml tRNA, and 100 µg/ml bovine serum albumin [BSA]) in PBT and then to 100% HB. Finally, intestines were transferred to warm HB for 2 h at 56°C and then incubated in 100 µl of HB containing 200 ng of digoxigenin (DIG)-labeled RNA probe overnight at 56°C. Day 2: Tissues were successively washed in warm 75%, 50%, 25%, and 0% HB in PBT for 15 min at 56°C. Endogenous peroxidases were quenched using 1% H_2O_2, and tissues were blocked in PBT containing 100 µg/ml BSA for 10 min at RT before incubation with horseradish peroxidase (HRP)-conjugated anti-DIG antibody (1/400) for 2 h at RT. Intestines were washed five times in PBS for 5 min each at RT. A TSA Cyanine 3 Signal Amplification System (#SAT704A001EA; Perkin Elmer) was used for signal detection according to the manufacturer's instructions. The *Drosophila Rab21* RNA probe was produced from an RT-PCR library generated from adult *Drosophila*, using the following primers: Fwd-5′-AGATG AATTCTCCCTGGAGGATGGGAGAAG-3′, Rev-5′-GCTAGAATTCG TATCCGGATTCTGGAGGC-3′. The following reagents were used for RNA probe synthesis and purification: T7 RNA polymerase (#10881767001; Roche), DIG RNA labeling mix (#11277073910; Roche), RNase inhibitor (#3335399001; Roche), and ProbeQuant G-50 Micro columns (#GE28-9034-08; Sigma).

SYTOX staining

SYTOX Orange Nucleic Acid Stain (#S11368; Thermo Fisher Scientific) was diluted to 1 µM in 5% sucrose and fed to the flies overnight. Fly guts were then dissected in 1× PBS, incubated for 10 min in cold 1× PBS containing Hoechst, and briefly rinsed in 1× PBS.

Intestines were mounted in SlowFade Gold Antifade Mountant with DAPI and imaged immediately.

Confocal microscopy

Confocal images of guts were acquired on a Zeiss LSM 880 confocal microscope, using either a 20 × Plan-APOCHROMAT/0.8 numerical aperture (NA) or a 40 × oil Plan APOCHROMAT/1.4 NA objective. Confocal images are presented as maximum projections. Settings on the microscope were first adjusted on a control gut and maintained for the acquisition of the different conditions in each experiment. Images were analyzed in Fiji (Schindelin *et al.*, 2012) or Cell-Profiler (Jones *et al.*, 2008) and then linearly thresholded and assembled into figure panels in Photoshop Version 21.1.1 (Adobe Systems, San Jose, CA). All adjustments to contrast and other aspects of the images were performed similarly for all conditions in each experiment.

TEM

Guts were dissected in 1× PBS, and posterior midguts were fixed with a 2.5% glutaraldehyde fixation solution in 0.1 M cacodylate buffer (pH 7.4) at 4°C overnight. Tissues were transferred into 10–25 µl of HistoGel (#HG-4000-012; Thermo Scientific), washed in 0.1 M cacodylate buffer (pH 7.4), and postfixed in 1% osmium tetroxide in 0.1 M cacodylate buffer. Guts were stained in 1% uranyl acetate overnight, dehydrated in successive 70%, 85%, 95%, and 100% ethanol baths, incubated in propylene oxide, and finally embedded in epoxy resin. Sections were mounted on copper grids and poststained with lead citrate. Images were acquired on a Hitachi H-7500 transmission electron microscope with an accelerating voltage of 80 keV. Images were analyzed in Fiji and thresholded in Photoshop.

Intestine RNA extraction and qRT-PCR

Guts (15–20) were quickly dissected in cold 1× PBS and transferred to TRIzol Reagent (#15596026; Invitrogen). RNA extractions were performed as described in the TRIzol Reagent protocol. RNA (500 ng) was reverse transcribed using the Maxima First Strand cDNA Synthesis kit (#K1671; Thermo Fisher Scientific). Primer sequences used for qRT-PCR were hid Fwd-5′-CCCAGCCAACGATTTTTATG-3′, hid Rev-5′-TGTTACCGCTCCGGCTAC-3′, Mkp3 Fwd-5′-TGGACT-CCATCATCAGCATCC-3′, Mkp3 Rev-5′-CGGTTTGAACATTGCG-ACTAG-3′, argos Fwd-5′-CCGGTGCATAAGTTGCCAGT-3′, argos Rev-5′-GCTTTCGCACCGTGAACAAT-3′, Actin5C Fwd-5′-CTC-GCCACTTGCGTTTACAGT-3′, and Actin Rev-5′-TCCATATCGT-CCCAGTTGGTC-3′. Relative mRNA levels were calculated using the $2^{-\Delta\Delta Ct}$ method (Livak and Schmittgen, 2001). ΔCt values were obtained by normalizing to actin.

Intestine protein extraction

Intestines (15–20) were quickly dissected in cold 1× PBS containing 1× protease inhibitor (#P8340; Sigma-Aldrich) and transferred into 1× SDS loading buffer prepared by mixing 4× SDS loading buffer (200 mM Tris, pH 6.8, 8% SDS, 1 mM dithiothreitol [DTT], 30% glycerol) with 1× lysis buffer (50 mM Tris, pH 7.5, 150 mM NaCl, 1 mM EDTA, 1% Triton X-100) at a 1:3 ratio and then adding 1× protease inhibitor. Tissue samples were dissociated using a syringe and boiled for 5 min at 95°C. Protein extracts were incubated for 15 min on ice and then centrifuged at 16,000 × g for 15 min at 4°C. Supernatants were then transferred to new tubes, and protein amounts were quantified by BCA assay (#23225; Pierce). For immunoblots, protein extracts were resolved by 12% SDS–PAGE and transferred to polyvinylidene difluoride membranes (#10600021; GE Healthcare).

Survival curves

Flies were grown at 18°C and collected 1–3 d after eclosion, incubated at 29°C on normal food, and aged until death. Dead flies were scored every 2–3 d, and food was exchanged every other day.

Smurf assays

Flies (1–3 d old) were collected in a tube and incubated at 29°C for 20 d. They were then transferred overnight to food containing FD&C blue dye #1 (1.75 g/100 ml). The next day, blue flies were scored as Smurf[+]. For positive control, blue food was supplemented with 5% SDS.

Circulating sugar and lipid quantifications

To collect hemolymph, at least 20 flies were pierced in the thorax using a 26G needle and collected in a 0.5 ml PCR tube that was pierced at the bottom. The PCR tube was placed into a 1.5 ml Eppendorf tube and centrifuged at $9000 \times g$ for 5 min at 4°C.

For sugar quantification (Galenza and Foley, 2021), 1 μl of hemolymph was diluted in 99 μl of trehalase buffer (5 mM Tris, pH 6.6, 137 mM NaCl, 2.7 mM KCl) and heated at 70°C for 5 min. Samples were split into two aliquots of 50 μl to measure circulating glucose (aliquot #1) and total circulating sugar (aliquot #2). Trehalase enzyme solution (50 μl; 1 U of porcine trehalase in 1 ml of trehalase buffer) was added to aliquot #2 to reach a total amount of 100 μl. In aliquot #1, 50 μl of trehalase buffer was added. Samples were incubated for 24 h at 37°C. For each aliquot, triplicate 30 μl samples were added to a 96-well plate and glucose was measured using the Glucose GO assay kit (GAGO20; Sigma). Absorbance was measured at 540 nm using a VersaMax Microplate Reader (Molecular Devices). Quantification from aliquot #1 refers to the total circulating sugar while aliquot #2 refers to circulating glucose. The circulating trehalose concentration was obtained by subtracting circulating glucose from total circulating sugars.

For mono/di/triglyceride quantification, 2 μl of hemolymph was diluted in 98 μl of water and heated at 70°C for 5 min. Quantification was performed using a Triglyceride Quantification Colorimetric Kit (#MAK266-T; Sigma) following the manufacturer's instructions. Absorbance was measured at 570 nm on a VersaMax Microplate Reader.

Image quantification

All analyses were performed in the distal part of the posterior midgut (R5) unless otherwise mentioned. The percentage of pH3^{+} cells was assessed as the total number of pH3^{+} cells in the region of interest divided by the total number of cells (revealed using DAPI staining) in the same region. Signal intensities were measured using the "Measure Image Intensity" module in CellProfiler. Normalized intensity signals correspond to signal intensities normalized by the mean of the signal intensities of controls from the same experiment.

Statistical analysis

Unpaired two-tailed Student's t tests and Mann–Whitney U tests were used to analyze significant differences between pairs of conditions. The proper statistical test for each experiment was determined by assessing the normal distributions of each condition in the experiment. Conditions with normal distributions were analyzed using unpaired two-tailed Student's t tests, while conditions without normal distributions were analyzed using Mann–Whitney U tests. Multiple conditions were analyzed by one-way analysis of variance (ANOVA) followed by Dunnett's test. All statistical comparisons were performed using data collected from at least three biological replicates, unless otherwise specified. GraphPad Prism (GraphPad Software, La Jolla, CA) was used for statistical analyses and graph generation. In graphs, scattered puncta correspond to biological samples (n) arising from three independent experiments (N), unless otherwise specified in the figure legends.

Protein processing for TMT-based proteomic analysis

Gut proteins were extracted as described above, using the same lysis buffer. Following gut dissection and protein extraction, biological replicates were flash frozen and simultaneously processed for TMT labeling. Proteins (50 μg) were reduced in 10 mM DTT for 2 min and then boiled and alkylated in 50 mM iodoacetamide for 30 min in the dark. DTT- and β-mercaptoethanol–free SDS loading buffer was added to the protein extracts to a final concentration of 1×. Proteins were resolved on 4–15% Mini-PROTEAN TGX Precast Protein Gels (#4561084; Bio-Rad) for 15 min at 200 V and visualized using SimplyBlue SafeStain solution (#LC6060; Thermo Fisher Scientific). For each condition, all proteins were loaded and contained in a single lane. The lane was excised from the gel and cut into two parts (higher and lower molecular weights); this step was performed to increase the number of detected proteins by MS. Gel bands were successively washed with 300 μl of H_2O and 300 μl of 100% acetonitrile (ACN) for 15 min each at RT. The supernatants were removed, and the gel bands were successively washed in 300 μl of 50 mM triethylammonium bicarbonate (TEAB) and 300 μl of 50:50 ACN:50 mM TEAB at RT for 15 min each. Supernatants were discarded, and the two washes were repeated if the gel bands remained blue. Finally, the gel bands were incubated in 150 μl of 100% ACN for 5 min at RT and dried for 5 min in a SpeedVac Vacuum Concentrator (Thermo Fisher Scientific). In-gel digestion was performed overnight in 50 μl reactions containing 12.5 ng/μl trypsin in 50 mM TEAB at 30°C. Digested gel bands were incubated in 50 μl of ACN for 30 min at RT. Supernatants containing digested peptides were collected, and residual peptides were eluted with 100% ACN and 1% formic acid. Peptides were dried and resuspended in 50 mM TEAB, and their concentrations were measured with a NanoDrop spectrophotometer (Thermo Fisher Scientific) using their absorbance at 205 nm. Finally, we performed TMT labeling using a TMT10plex Isobaric Label Reagent Set (#90110; Thermo Fisher Scientific) according to the manufacturer's protocol, using the same maximal quantity of peptides for each condition. Peptides from bands A and B from the same condition were independently labeled with the same label. Labeled peptides from all band A samples from the different conditions were pooled, as were the labeled peptides from all band B samples. The pooled samples were dried, resuspended in 0.1% trifluoroacetic acid diluted in water, and desalted using a ZipTip. For each pooled sample, 1.5 μg peptides were resuspended in 1% formic acid diluted in water and loaded on a Q Exactive Orbitrap mass spectrometer (Thermo Fisher Scientific). Settings used were as previously described (Del Olmo et al., 2019), except that the full-scan MS survey spectra acquisition (m/z 375–1400) was realized using a resolution of 140,000 with 3,000,000 ions and a maximum injection time of 120 ms.

MS data analysis

For the TMT-based quantitative proteomic experiment, three independent biological replicates were used. Proteins were identified by MaxQuant using the UniProt Drosophila melanogaster proteome UP000000803. The "proteinGroup.txt" output file from the MaxQuant analysis (Cox and Mann, 2008) (Supplemental Table 1) was used to collect corrected reporter intensities per sample for every detected protein, as a measure of their quantities in each sample.

Because individual replicates were run on different days, we checked for the presence of batch effects by generating a multidimensional scaling plot using the limma v3.42.2 package (Ritchie *et al.*, 2015) in the R environment. Once confirmed, batch effects were handled in R using the internal reference scaling (IRS) methodology (Plubell *et al.*, 2017), which can correct the random MS2 sampling that occurs between TMT experiments. Because the data set contained proteins that were not quantified in all replicates, we first filtered for proteins identified in two of three replicates of at least one condition and then checked the spectra for missing data using the DEP v1.8.0 R package (Zhang *et al.*, 2018). Once we verified that missing data were occurring at random, we imputed them using the k-nearest neighbor approach in DEP v1.8.0. Following this analysis, only proteins with two unique peptides were conserved for data representation (Figure 7B) and Reactome enrichment analysis (Figure 7C). Differential expression analysis was performed in R using DEP v1.8.0, with a false discovery rate (FDR) of 0.05 and a $\log_2$ fold change (FC) of 1.5. Enriched Reactome pathways were independently searched for proteins with >2-fold increases or decreases in abundance using the "STRING enrichment "plug-in in Cytoscape (Shannon *et al.*, 2003). The MS data have been deposited to the ProteomeXchange Consortium via the PRIDE repository with the data set identifier PXD022413.

REFERENCES

Amcheslavsky A, Jiang J, Ip YT (2009). Tissue damage-induced intestinal stem cell division in Drosophila. Cell Stem Cell 4, 49–61.

Ayyadurai S, Charania MA, Xiao B, Viennois E, Merlin D (2013). PepT1 expressed in immune cells has an important role in promoting the immune response during experimentally induced colitis. Lab Investig 93, 888–899.

Beebe K, Lee WC, Micchelli CA (2010). JAK/STAT signaling coordinates stem cell proliferation and multilineage differentiation in the Drosophila intestinal stem cell lineage. Dev Biol 338, 28–37.

Buchon N, Broderick NA, Chakrabarti S, Lemaitre B (2009). Invasive and indigenous microbiota impact intestinal stem cell activity through multiple pathways in Drosophila. Genes Dev 23, 2333–2344.

Buchon N, Broderick NA, Kuraishi T, Lemaitre B (2010). Drosophila EGFR pathway coordinates stem cell proliferation and gut remodeling following infection. BMC Biol 8, 152.

Buchon N, Osman D, David FPA, Yu Fang H, Boquete JP, Deplancke B, Lemaitre B (2013). Morphological and molecular characterization of adult midgut compartmentalization in Drosophila. Cell Rep 3, 1725–1738.

Carlson JC, Weeks DE, Hawley NL, Sun G, Cheng H, Naseri T, Reupena MS, Tuitele J, Deka R, McGarvey S, et al. (2021). Genome-wide association studies in Samoans give insight into the genetic architecture of fasting serum lipid levels. J Hum Genet 66, 111–121.

Chan CC, Scoggin S, Wang D, Cherry S, Dembo T, Greenberg B, Jin EJ, Kuey C, Lopez A, Mehta SQ, et al. (2011). Systematic discovery of Rab GTPases with synaptic functions in Drosophila. Curr Biol 21, 1704–1715.

Chen HJ, Li Q, Nirala NK, Ip YT (2020). The snakeskin-mesh complex of smooth septate junction restricts Yorkie to regulate intestinal homeostasis in Drosophila. Stem Cell Rep 14, 828–844.

Cox J, Mann M (2008). MaxQuant enables high peptide identification rates, individualized p.p.b.-range mass accuracies and proteome-wide protein quantification. Nat Biotechnol. 26, 1367–1372.

Cullen PJ, Steinberg F (2018). To degrade or not to degrade: mechanisms and significance of endocytic recycling. Nat Rev Mol Cell Biol 19, 679–696.

D'Agostino L, Nie Y, Goswami S, Tong K, Yu S, Bandyopadhyay S, Flores J, Zhang X, Balasubramanian I, Joseph I, et al. (2019). Recycling endosomes in mature epithelia restrain tumorigenic signaling. Cancer Res 79, 4099–4112.

Del Olmo T, Lauzier A, Normandin C, Larcher R, Lecours M, Jean D, Lessard L, Steinberg F, Boisvert F, Jean S (2019). APEX2-mediated RAB proximity labeling identifies a role for RAB21 in clathrin-independent cargo sorting. EMBO Rep 20, e47192.

Du G, Qiao Y, Zhuo Z, Zhou J, Li X, Liu Z, Li Y, Chen H (2020). Lipoic acid rejuvenates aged intestinal stem cells by preventing age-associated endosome reduction. EMBO Rep 21, 1–24.

Dutta D, Dobson AJ, Houtz PL, Gläßer C, Revah J, Korzelius J, Patel PH, Edgar BA, Buchon N (2015). Regional cell-specific transcriptome mapping reveals regulatory complexity in the adult Drosophila midgut. Cell Rep 12, 346–358.

Eckel RH, Grundy SM, Zimmet PZ (2005). The metabolic syndrome. Lancet 365, 1415–1428.

Engevik AC, Goldenring JR (2018). Trafficking ion transporters to the apical membrane of polarized intestinal enterocytes. Cold Spring Harb Perspect Biol 10, 1–16.

Feng Q, Bonder EM, Engevik AC, Zhang L, Tyska MJ, Goldenring JR, Gao N (2017). Disruption of Rab8a and Rab11a causes formation of basolateral microvilli in neonatal enteropathy. J Cell Sci 130, 2491–2505.

Galenza A, Foley E (2021). A glucose-supplemented diet enhances gut barrier integrity in Drosophila. Biol Open 10, bio056515.

Galvez T, Gilleron J, Zerial M, O'Sullivan GA (2012). SnapShot: mammalian Rab proteins in endocytic trafficking. Cell 151, 234.e2.

Henne WM, Buchkovich NJ, Emr SD (2011). The ESCRT pathway. Dev Cell 21, 77–91.

Houtz P, Bonfini A, Liu X, Revah J, Guillou A, Poidevin M, Hens K, Huang H-Y, Deplancke B, Tsai Y-C, et al. (2017). Hippo, TGF-β, and Src-MAPK pathways regulate transcription of the upd3 cytokine in Drosophila enterocytes upon bacterial infection. PLoS Genet 13, e1007091.

Hutagalung AH, Novick PJ (2011). Role of Rab GTPases in membrane traffic and cell physiology. Physiol Rev 91, 119–149.

Jean S, Cox S, Nassari S, Kiger AA (2015). Starvation-induced MTMR13 and RAB21 activity regulates VAMP8 to promote autophagosome-lysosome fusion. EMBO Rep 16, 297–311.

Jean S, Cox S, Schmidt EJ, Robinson FL, Kiger A (2012). Sbf/MTMR13 coordinates PI(3)P and Rab21 regulation in endocytic control of cellular remodeling. Mol Biol Cell 23, 2723–2740.

Jean S, Kiger AA (2012). Coordination between RAB GTPase and phosphoinositide regulation and functions. Nat Rev Mol Cell Biol 13, 463–470.

Jiang H, Edgar BA (2011). Intestinal stem cells in the adult Drosophila midgut. Exp Cell Res 317, 2780–2788.

Jiang H, Grenley MO, Bravo MJ, Blumhagen RZ, Edgar BA (2011). EGFR/Ras/MAPK signaling mediates adult midgut epithelial homeostasis and regeneration in drosophila. Cell Stem Cell 8, 84–95.

Jiang H, Patel PH, Kohlmaier A, Grenley MO, McEwen DG, Edgar BA (2009). Cytokine/Jak/Stat signaling mediates regeneration and homeostasis in the Drosophila midgut. Cell 137, 1343–1355.

Jones TR, Kang IH, Wheeler DB, Lindquist RA, Papallo A, Sabatini DM, Golland P, Carpenter AE (2008). CellProfiler Analyst: data exploration

and analysis software for complex image-based screens. BMC Bioinform 9, 482.

Kanamori Y, Saito A, Hagiwara-Komoda Y, Tanaka D, Mitsumasu K, Kikuta S, Watanabe M, Cornette R, Kikawada T, Okuda T (2010). The trehalose transporter 1 gene sequence is conserved in insects and encodes proteins with different kinetic properties involved in trehalose import into peripheral tissues. Insect Biochem Mol Biol 40, 30–37.

Knowles BC, Weis VG, Yu S, Roland JT, Williams JA, Alvarado GS, Lapierre LA, Shub MD, Gao N, Goldenring JR (2015). Rab11a regulates syntaxin 3 localization and microvillus assembly in enterocytes. J Cell Sci 128, 1617–1626.

Lauzier A, Normandeau-Guimond J, Vaillancourt-Lavigueur V, Boivin V, Charbonneau M, Rivard N, Scott MS, Dubois CM, Jean S (2019). Colorectal cancer cells respond differentially to autophagy inhibition in vivo. Sci Rep 9, 11316.

Li Q, Nirala NK, Nie Y, Chen HJ, Ostroff G, Mao J, Wang Q, Xu L, Ip YT (2018). Ingestion of food particles regulates the mechanosensing Misshapen-Yorkie pathway in Drosophila intestinal growth. Dev Cell 45, 433–449.e6.

Liang J, Balachandra S, Ngo S, O'Brien LE (2017). Feedback regulation of steady-state epithelial turnover and organ size. Nature 548, 588–591.

Lin G, Xi R (2008). Intestinal stem cell, muscular niche and wingless signaling. Fly (Austin) 2, 310–312.

Lin G, Xu N, Xi R (2008). Paracrine Wingless signalling controls self-renewal of Drosophila intestinal stem cells. Nature 455, 1119–1123.

Lin G, Xu N, Xi R (2010). Paracrine unpaired signaling through the JAK/STAT pathway controls self-renewal and lineage differentiation of Drosophila intestinal stem cells. J Mol Cell Biol 2, 37–49.

Livak KJ, Schmittgen TD (2001). Analysis of relative gene expression data using real-time quantitative PCR and the 2-ΔΔCT method. Methods 25, 402–408.

Loudhaief R, Brun-Barale A, Benguettat O, Nawrot-Esposito M-P, Pauron D, Amichot M, Gallet A (2017). Apoptosis restores cellular density by eliminating a physiologically or genetically induced excess of enterocytes in the Drosophila midgut. Development 144, 808–819.

Lu H, Bilder D (2005). Endocytic control of epithelial polarity and proliferation in Drosophila. Nat Cell Biol 7, 1132–1139.

Marianes A, Spradling AC (2013). Physiological and stem cell compartmentalization within the Drosophila midgut. eLife 2, e00886.

Mattila J, Hietakangas V (2017). Regulation of carbohydrate energy metabolism in Drosophila melanogaster. Genetics 207, 1231–1253.

McGuire SE, Mao Z, Davis RL (2004). Spatiotemporal gene expression targeting with the TARGET and gene-switch systems in Drosophila. Sci STKE 2004, 1–11.

Melendez J, Liu M, Sampson L, Akunuru S, Han X, Vallance J, Witte D, Shroyer N, Zheng Y (2013). Cdc42 coordinates proliferation, polarity, migration, and differentiation of small intestinal epithelial cells in mice. Gastroenterology 145, 808–819.

Micchelli CA, Perrimon N (2006). Evidence that stem cells reside in the adult Drosophila midgut epithelium. Nature 439, 475–479.

Michaux G, Massey-Harroche D, Nicolle O, Rabant M, Brousse N, Goulet O, Le Bivic A, Ruemmele FM (2016). The localisation of the apical Par/Cdc42 polarity module is specifically affected in microvillus inclusion disease. Biol Cell 108, 19–28.

Miguel-Aliaga I, Jasper H, Lemaitre B (2018). Anatomy and physiology of the digestive tract of drosophila melanogaster. Genetics 210, 357–396.

Misra JR, Irvine KD (2018). The hippo signaling network and its biological functions. Annu Rev Genet 52, 65–87.

Moreno-Layseca P, Jäntti NZ, Godbole R, Sommer C, Jacquemet G, Al-Akhrass H, Conway JRW, Kronqvist P, Kallionpää RE, Oliveira-Ferrer L, et al. (2021). Cargo-specific recruitment in clathrin- and dynamin-independent endocytosis. Nat Cell Biol 2021, 1073–1084.

Morrison HA, Dionne H, Rusten TE, Brech A, Fisher WW, Pfeiffer BD, Celniker SE, Stenmark H, Bilder D (2008). Regulation of early endosomal entry by the Drosophila tumor suppressors rabenosyn and Vps45. Mol Biol Cell 19, 4167–4176.

Müller T, Hess MW, Schiefermeier N, Pfaller K, Ebner HL, Heinz-Erian P, Ponstingl H, Partsch J, Röllinghoff B, Köhler H, et al. (2008). MYO5B mutations cause microvillus inclusion disease and disrupt epithelial cell polarity. Nat Genet. 40, 1163–1165.

Nagai H, Tatara H, Tanaka-Furuhashi K, Kurata S, Yano T (2021). Homeostatic regulation of ROS-triggered Hippo-Yki pathway via autophagic clearance of Ref(2)P/p62 in the Drosophila intestine. Dev Cell 56, 81–94.

Nassari S, Olmo TD, Jean S (2020). Rabs in signaling and embryonic development. Int J Mol Sci 21, 1064.

Nie Y, Yu S, Li Q, Nirala NK, Amcheslavsky A, Edwards YJK, Shum PW, Jiang Z, Wang W, Zhang B, et al. (2019). Oncogenic pathways and loss of the Rab11 GTPase synergize to alter metabolism in Drosophila. Genetics 212, 1227–1239.

Ohlstein B, Spradling A (2006). The adult Drosophila posterior midgut is maintained by pluripotent stem cells. Nature 439, 470–474.

Opdam FJM, Kamps G, Croes H, Van Bokhoven H, Ginsel LA, Fransen JAM (2000). Expression of Rab small GTPases in epithelial Caco-2 cells: Rab21 is an apically located GTP-binding protein in polarised intestinal epithelial cells. Eur J Cell Biol 79, 308–316.

Palm W, Sampaio JL, Brankatschk M, Carvalho M, Mahmoud A (2012). Lipoproteins in Drosophila melanogaster—assembly, function, and influence on tissue lipid composition. PLoS Genet 8, 1002828.

Patel PH, Dutta D, Edgar BA (2015). Niche appropriation by Drosophila intestinal stem cell tumours. Nat Cell Biol 17, 1182–1192.

Patel PH, Pénalva C, Kardorff M, Roca M, Pavlovi B, Thiel A, Teleman AA, Edgar BA (2019). Damage sensing by a Nox-Ask1-MKK3-p38 signaling pathway mediates regeneration in the adult Drosophila midgut. Nat Commun 10, 1–14.

Pellinen T, Arjonen A, Vuoriluoto K, Kallio K, Fransen JAM, Ivaska J (2006). Small GTPase Rab21 regulates cell adhesion and controls endosomal traffic of β1-integrins. J Cell Biol 173, 767–780.

Plubell DL, Wilmarth PA, Zhao Y, Fenton AM, Minnier J, Reddy AP, Klimek J, Yang X, David LL, Pamir N (2017). Extended multiplexing of tandem mass tags (TMT) labeling reveals age and high fat diet specific proteome changes in mouse epididymal adipose tissue. Mol Cell Proteom 16, 873–890.

Pulipparacharuvil S (2005). Drosophila Vps16A is required for trafficking to lysosomes and biogenesis of pigment granules. J Cell Sci 118, 3663–3673.

Ren F, Wang B, Yue T, Yun EY, Ip YT, Jiang J (2010). Hippo signaling regulates Drosophila intestine stem cell proliferation through multiple pathways. Proc Natl Acad Sci USA 107, 21064–21069.

Ritchie ME, Phipson B, Wu D, Hu Y, Law CW, Shi W, Smyth GK (2015). Limma powers differential expression analyses for RNA-sequencing and microarray studies. Nucleic Acids Res. 43, e47.

Sakamori R, Das S, Yu S, Feng S, Stypulkowski E, Guan Y, Douard V, Tang W, Ferraris RP, Harada A, et al. (2012). Cdc42 and Rab8a are critical for intestinal stem cell division, survival, and differentiation in mice. J Clin Invest 122, 1052–1065.

Sané AT, Seidman E, Peretti N, Kleme ML, Delvin E, Deslandres C, Garofalo C, Spahis S, Levy E (2017). Understanding chylomicron retention disease through Sar1B Gtpase gene disruption: insight from cell culture. Arterioscler Thromb Vasc Biol 37, 2243–2251

Sato T, Mushiake S, Kato Y, Sato K, Sato M, Takeda N, Ozono K, Miki K, Kubo Y, Tsuji A, et al. (2007). The Rab8 GTPase regulates apical protein localization in intestinal cells. Nature 448, 366–369.

Schindelin J, Arganda-Carreras I, Frise E, Kaynig V, Longair M, Pietzsch T, Preibisch S, Rueden C, Saalfeld S, Schmid B, et al. (2012). Fiji: an open-source platform for biological-image analysis. Nat Methods. 9, 676–682.

Shannon P, Markiel A, Ozier O, Baliga NS, Wang JT, Ramage D, Amin N, Schwikowski B, Ideker T (2003). Cytoscape: a software environment for integrated models of biomolecular interaction networks. Genome Res 13, 2498–2504.

Shaw RL, Kohlmaier A, Polesello C, Veelken C, Edgar BA, Tapon N (2010). The Hippo pathway regulates intestinal stem cell proliferation during Drosophila adult midgut regeneration. Development 137, 4147–4158.

Shin H-W, Hayashi M, Christoforidis S, Lacas-Gervais S, Hoepfner S, Wenk MR, Modregger J, Uttenweiler-Joseph S, Wilm M, Nystuen A, et al. (2005). An enzymatic cascade of Rab5 effectors regulates phosphoinositide turnover in the endocytic pathway. J Cell Biol 170, 607–618.

Staley BK, Irvine KD (2010). Warts and yorkie mediate intestinal regeneration by influencing stem cell proliferation. Curr Biol 20, 1580–1587.

Turcot V, Lu Y, Highland HM, Schurmann C, Justice AE, Fine RS, Bradfield JP, Esko T, Giri A, Graff M, et al. (2018). Protein-altering variants associated with body mass index implicate pathways that control energy intake and expenditure in obesity. Nat Genet. 50, 26–41.

Viennois E, Ingersoll SA, Ayyadurai S, Zhao Y, Wang L, Zhang M, Han MK, Garg P, Xiao B, Merlin D (2016). Critical role of PepT1 in promoting colitis-associated cancer and therapeutic benefits of the anti-inflammatory PepT1-mediated tripeptide KPV in a murine model. Cell Mol Gastroenterol Hepatol 2, 340–357.

Volkenhoff A, Weiler A, Letzel M, Stehling M, Klämbt C, Schirmeier S (2015). Glial glycolysis is essential for neuronal survival in drosophila. Cell Metab 22, 437–447.

Wiegerinck CL, Janecke AR, Schneeberger K, Vogel GF, van Haaften-Visser DY, Escher JC, Adam R, Thöni CE, Pfaller K, Jordan AJ, et al. (2014). Loss of syntaxin 3 causes variant microvillus inclusion disease. Gastroenterology 147, 65–68.e10.

Winter JF, Höpfner S, Korn K, Farnung BO, Bradshaw CR, Marsico G, Volkmer M, Habermann B, Zerial M (2012). Caenorhabditis elegans screen reveals role of PAR-5 in RAB-11-recycling endosome positioning and apicobasal cell polarity. Nat Cell Biol 14, 666–676.

Wucherpfennig T, Wilsch-Bräuninger M, González-Gaitán M (2003). Role of Drosophila Rab5 during endosomal trafficking at the synapse and evoked neurotransmitter release. J Cell Biol 161, 609–624.

Xu C, Tang HW, Hung RJ, Hu Y, Ni X, Housden BE, Perrimon N (2019). The septate junction protein Tsp2A restricts intestinal stem cell activity via endocytic regulation of aPKC and Hippo signaling. Cell Rep 26, 670–688.e6.

Yang X, Zhang Y, Li S, Liu C, Jin Z, Wang Y, Ren F, Chang Z (2012). Rab21 attenuates EGF-mediated MAPK signaling through enhancing EGFR internalization and degradation. Biochem Biophys Res Commun 421, 651–657.

Yarwood R, Hellicar J, Woodman PG, Lowe M (2020). Membrane trafficking in health and disease. Dis Model Mech 13, dmm043448.

Yu S, Nie Y, Knowles B, Sakamori R, Stypulkowski E, Patel C, Das S, Douard V, Ferraris RP, Bonder EM, et al. (2014). TLR sorting by Rab11 endosomes maintains intestinal epithelial-microbial homeostasis. EMBO J 33, 1882–1895.

Zeigerer A, Gilleron J, Bogorad RL, Marsico G, Nonaka H, Seifert S, Epstein-Barash H, Kuchimanchi S, Peng CG, Ruda VM, et al. (2012). Rab5 is necessary for the biogenesis of the endolysosomal system in vivo. Nature 485, 465–470.

Zhang P, Holowatyj AN, Roy T, Pronovost SM, Marchetti M, Liu H, Ulrich CM, Edgar BA (2019). An SH3PX1-dependent endocytosis-autophagy network restrains intestinal stem cell proliferation by counteracting EGFR-ERK signaling. Dev Cell 49, 574–589.e5.

Zhang X, Smits AH, Van Tilburg GBA, Ovaa H, Huber W, Vermeulen M (2018). Proteome-wide identification of ubiquitin interactions using UbIA-MS. Nat Protoc. 13, 530–550.

Zhang Y, Viennois E, Zhang M, Xiao B, Han MK, Walter L, Garg P, Merlin D (2016). PepT1 expression helps maintain intestinal homeostasis by mediating the differential expression of miRNAs along the crypt-villus axis. Sci Rep 6, 1–21.

Zhao S, Xia J, Wu X, Zhang L, Wang P, Wang H, Li H, Wang X, Chen Y, Agnetti J, et al. (2018). Deficiency in class III PI3-kinase confers postnatal lethality with IBD-like features in zebrafish. Nat Commun 9, 1–13.

Zhou J, Valentini E, Boutros M (2021). Microenvironmental innate immune signaling and cell mechanical responses promote tumor growth. Dev Cell 56, 1884–1899.e5